PHILOSOPHICAL TRANSACTIONS OF THE ROYAL SOCIETY A MATHEMATICAL, PHYSICAL & ENGINEERING SCIENCES

The Lubrication of Rollers IV. Measurements of Friction and Effective Viscosity

A. W. Crook

Phil. Trans. R. Soc. Lond. A 1963 **255**, 281-312
doi: 10.1098/rsta.1963.0005

THE LUBRICATION OF ROLLERS

IV. MEASUREMENTS OF FRICTION AND EFFECTIVE VISCOSITY

By A. W. CROOK

Research Laboratory, Associated Electrical Industries, Aldermaston Court, Aldermaston, Berkshire

(*Communicated by T. E. Allibone, F.R.S.—Received* 20 *December* 1961—
Read 5 *April* 1962—*Revised* 18 *May* 1962)

CONTENTS

Measurements of friction with disk machines are described. The measurements have been made under conditions which fit them particularly for comparison with the theory of hydrodynamic lubrication of rollers and with the theory of frictional heating which has been developed in part III. The frictions due to rolling and sliding have been measured separately.

It is shown that the frictional tractions T_1 and T_2 acting upon the surfaces of two disks can be expressed by

$$T_{1,2} = T_R \mp T_S,$$

where T_R is the traction due to rolling and T_S is that due to sliding. If the disk 1 runs freely in frictionless bearings T_1 must be zero and the disk runs in the condition

$$T_R = T_S.$$

Vol. 255. A. 1056. (Price 10*s*.) 36 [Published 17 January 1963

A four-disk machine is described in which the central disk, since it has no bearings, runs in the above condition unless some external torque is imposed upon it. External torques were applied by a band brake and from the curves of traction against sliding thereby obtained both T_R and the way in which T_S increases with sliding speed were deduced.

It is shown that in the elasto-hydrodynamic régime T_R is independent of load and simply proportional to the thickness of the hydrodynamic film. It is also shown that this behaviour follows from the hydrodynamic theory and that the magnitudes of the rolling friction as predicted by theory and as deduced from experiment are substantially in accord.

From experimental determinations of film thickness and from the linear increase of T_S with sliding speed over the range of sliding speeds employed (~ 1 cm s^{-1}) values of the effective viscosity ($\bar{\eta}_m$) at the rolling point were deduced and are presented as a function of rolling speed ($\bar{u} = \frac{1}{2}(u_1 + u_2)$). By effective viscosity is meant that constant viscosity throughout the conjunction of the disks which would give rise to the observed friction. It is shown that the values of $\bar{\eta}_m$ so obtained when extrapolated to zero rolling speed are consistent with published results of experiments with dropping ball viscometers in high-pressure apparatus (*Pressure Viscosity Report* 1953) both with respect to the effects of pressure and of temperature. But the more important feature of the results from the disk experiments is that they show the effects of pressure and temperature upon the apparent viscosity of the oil to diminish as the rolling speed is increased, i.e. as the time for which the oil is under stress diminishes. This behaviour is interpreted in terms of a Maxwellian fluid and the required values of the elastic modulus in shear are deduced. However, although the visco-elastic hypothesis accounts for the observations it is stressed that it cannot yet be taken as the definitive explanation.

In a further series of experiments a two-disk machine adapted for the direct measurement of friction independently of bearing frictions was used to explore sliding speeds up to 400 cm s^{-1}. In contrast with the previous measurements, at such speeds of sliding frictional heating has a major effect upon effective viscosity, for example, in a particular instance the introduction of 400 cm s^{-1} sliding caused the effective viscosity to fall from ~ 3000 P at the rolling point to ~ 20 P. It is shown that the frictions and effective viscosities predicted by the theory of frictional heating (part III) and the measurements now reported are, in their larger aspects, substantially in accord. For example, in a particular instance theory predicted a coefficient of friction of 0·05 whereas experiment gave a coefficient of 0·03 and both experiment and theory show that as the sliding speed increases the friction rises to a maximum and then falls.

But the theory of part III when applied to the experimental results leads to a value of the thermal conductivity of the oil of about half that to be expected from Bridgman's work (1949). However, measurements in finer detail of friction up to a sliding speed of 30 cm s^{-1} indicate that an intrinsic effect (i.e. an effect at constant temperature) of rate of strain upon viscosity exists. By taking this into account the anomaly with respect to thermal conductivity can be resolved.

The experimental results show clearly that in a lubricating system of widespread type (e.g. ball-races, gears) a mineral oil exhibits distinctive dynamic characteristics which are of significance with respect both to friction and to the thickness of the hydrodynamic oil film. The comparison of experiment and theory also emphasizes the importance of the thermal conductivity of the oil in relation to friction and to the temperatures in the oil film.

1. Introduction

Many measurements of the friction between gear teeth (see, for example, Cameron & Newman 1953) and of the friction between disks in a disk machine (see, for example, Misharin 1958) have been reported. Generally the measurements have been made with the purposes of knowing the friction and of finding empirically correlations with design parameters. But with the greater understanding of elasto-hydrodynamic lubrication now available, conditions can be set for measurements of friction which fit them particularly for comparison with physical theory. Measurements of friction made for such a comparison are described in this paper and the results are discussed in relation to the theory of

PHILOSOPHICAL TRANSACTIONS OF THE ROYAL SOCIETY A MATHEMATICAL, PHYSICAL & ENGINEERING SCIENCES

hydro-dynamic lubrication and to the theory of frictional heating developed in part III (Crook 1961 *b*).

The friction comprises a component due to the rolling of the disks and, if their peripheral speeds be unequal, a component due to their sliding. The rolling component arises from the curvature forced upon the velocity profiles by the convergence of the entry (figure 1 (*a*)) while the sliding component arises from the tilt superimposed upon the velocity profiles of figure 1 (*a*) by the sliding (figure 1 (*b*)). The rolling friction is small. Even though approximate allowance be made for bearing losses the rolling friction is easily obscured by bearing friction. Furthermore, the rolling friction may be exceeded by the friction due to small amounts of sliding which pass unobserved in conditions which would normally be regarded as pure rolling. However, with a disk machine of unconventional design it has been possible to measure the rolling friction. The results are compared with theory.

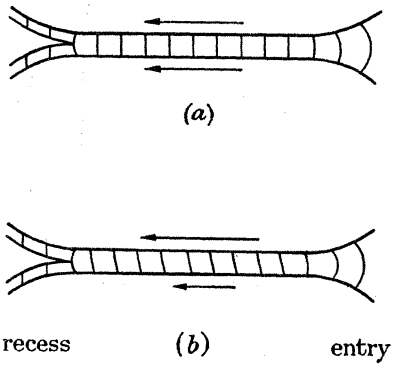

FIGURE 1. Velocity profiles. (*a*) Pure rolling, (*b*) with sliding.

The sliding friction, which arises predominantly from the parallel section of the conjunction (figure 1), depends upon the thickness of the hydrodynamic film, sliding speed and viscosity. From measurements of friction, thickness and sliding, an effective viscosity has been deduced. The actual viscosity (η) varies from point to point throughout the conjunction; the effective viscosity ($\bar{\eta}_m$) is that constant viscosity which would produce the observed friction.

The effects of pressure and temperature upon oil viscosity as measured under sustained stress are known from measurements in high-pressure apparatus (*Pressure Viscosity Report* 1953). However, the effects may not be the same under the transient stresses experienced by the oil in its passage through the conjunction of the disks. The importance of the effective viscosity is that it relates directly to that transient state.

Effective viscosities have been deduced from conditions near to pure rolling up to the inclusion of 400 cm s^{-1} sliding. Near the rolling point, because there is little frictional heating, it has been possible to detect a specific influence of rolling speed upon the effective viscosity. A tentative interpretation of the effect in terms of visco-elasticity is given. By the introduction of increasing amounts of sliding the influence of frictional heating upon effective viscosity has been followed. The results are compared with the theory of frictional heating already developed in part III (Crook 1961 *b*).

2. General expressions for rolling and sliding friction

The obvious way of considering the frictional traction is to equate it with the viscous drag at the surface of a disk. But close to and within the conjunction the normals to the surface of a disk will not in general pass through the axis of rotation. Consequently a possibility exists that a resultant moment due to the pressure contributes to the resistance to motion. To avoid this complication the tractions will be derived from the energy equation.

The rate of energy dissipation throughout the oil film is given by the volume integral of $\eta(\partial u/\partial y)^2$, where η is the local viscosity and u is the velocity of the oil (u will be taken positive in the negative direction of x, figure 2). Integration with respect to y gives

$$\int_0^h \eta \left(\frac{\partial u}{\partial y}\right)^2 \mathrm{d}y = \left[\eta u \frac{\partial u}{\partial y} - \int u \frac{\partial}{\partial y}\left(\eta \frac{\partial u}{\partial y}\right) \mathrm{d}y\right]_0^h, \tag{2·1}$$

where h is the gap separating the disks at x.

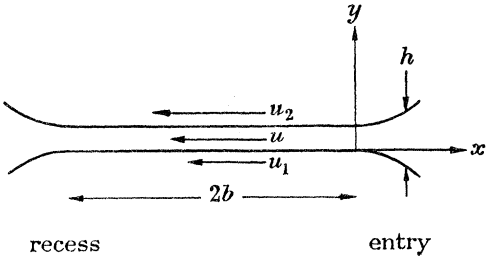

Figure 2. Co-ordinates.

In § 2 of part III the hydrodynamic equation was considered for the circumstance that η is a function not only of x but also of y. It was shown (equation (2·2) of part III) that

$$\frac{\partial u}{\partial y} = -\frac{1}{\eta}\frac{\partial P}{\partial x}\left(y - \frac{h}{m}\right) + \frac{\eta_m}{\eta}\frac{(u_2 - u_1)}{h}, \tag{2·2}$$

where P is pressure, η_m is the viscosity at $y = h/m$, $u_{1,2}$ are the peripheral speeds and m is defined by the place where $\partial u/\partial y = (u_2 - u_1)/h$. From equations (2·1) and (2·2) it may be seen that

$$\int_0^h \eta \left(\frac{\partial u}{\partial y}\right)^2 \mathrm{d}y = \left[\left(\eta u \frac{\partial u}{\partial y}\right)_{y=h} - \left(\eta u \frac{\partial u}{\partial y}\right)_{y=0} + \frac{\partial P}{\partial x}\int_0^h u \,\mathrm{d}y\right].$$

The integral on the right (the coefficient of $\partial P/\partial x$) is simply the rate of flow of oil and must be independent of x. Consequently, upon integrating with respect to x between limits where the pressures are zero (from $x = \infty$ to $x = -2b$) no contribution will arise from the term in $\partial P/\partial x$. It then follows that if W be the rate of dissipation of energy

$$W = \int_{-2b}^{\infty} \left(\eta u \frac{\partial u}{\partial y}\right)_{y=h} \mathrm{d}x - \int_{-2b}^{\infty} \left(\eta u \frac{\partial u}{\partial y}\right)_{y=0} \mathrm{d}x, \tag{2·3}$$

where $2b$ is the width of the parallel part of the conjunction (figure 2). Equation (2·3) shows that the tractions per unit face width (T),

$$T_1 = -\int_{-2b}^{\infty} \left(\eta \frac{\partial u}{\partial y}\right)_{y=0} \mathrm{d}x \quad \text{and} \quad T_2 = \int_{-2b}^{\infty} \left(\eta \frac{\partial u}{\partial y}\right)_{y=h} \mathrm{d}x$$

which arise from viscous drag at the surfaces by themselves satisfy W.

If the quantities

$$T_R = -\frac{1}{2}\int_{-2b}^{\infty} h\frac{\partial P}{\partial x}\,\mathrm{d}x, \quad T_S = (u_2 - u_1)\int_{-2b}^{\infty} \frac{\eta_m}{h}\,\mathrm{d}x \tag{2·4}$$

be defined it may be shown from equation (2·2) that

$$T_{1,2} = T_R \mp T_S \tag{2·5}$$

provided that m (equation (2·2)) has the value two as, by symmetry, it must have at the rolling point. Clearly T_R is the rolling friction and T_S is the friction due to sliding. (At values of sliding such that m can no longer be regarded as having the value two the expression for T_S (equation (2·4)) still stands but not that for T_R. Then the rolling frictions at the two surfaces are unequal. However, they are then small compared with T_S and consequently may be neglected.)

If the lower disk (figure 2) runs in frictionless bearings the traction T_1 must be zero. Contrary to common assumption, the disks will not roll but will run, so that

$$T_R = T_S.$$

3. Measurements near the rolling point

(*a*) *The four-disk machine*

To measure friction near to the rolling point a disk machine of the form shown in figure 3 (*a*) was built. The central disk which is supported entirely by the three outer disks, needs no bearings and consequently runs in the condition

$$T_R = T_S$$

unless some torque be intentionally imposed upon it.

The construction of the machine is illustrated by figure 3 (*b*). The disks A and B run in bearings in the machine frame (not shown) while disk C runs in self-alining races in the pair of loading arms. Axial location of the central disk (D) is provided by the air thrust block (E) which comprises a slotted block with a circular plate running in the slot. The block is drilled internally so that air can be pumped into both gaps (1×10^{-2} cm clearance) formed by the plate in the slot. The two air streams are both throttled by constrictions (1 mm bore, 9 mm long) which create a differential pressure tending to centre the plate should it move from the central position in the slot. Air is supplied at 20 Lb. in.$^{-2}$. An elementary calculation based upon laminar flow gave 2×10^{-2} dyn per rev/min at 3 in. diameter (nominal diameter of disk D) for the frictional traction due to the viscous drag of the air in the thrust. In the context of the experiments such a traction is imperceptible.

The outer disks (A, B and C) were lapped to be equal in diameter to within 2×10^{-5} cm and all are driven at equal speed by the gear train F. To obtain motions of the greatest possible uniformity the gears are helical and their teeth were ground.

All the disks are of case-hardened steel (750 V.p.n.) nominally of 3 in. diameter (7·6 cm) and were lapped so that their generators were straight to within 5×10^{-5} cm. The outer disks are of 1 in. (2·54 cm) face width while the central disk was relieved to leave a central track 0·75 in. (1·9 cm) wide.

The lapping technique was established with the central disk which as a result is of slightly smaller diameter than the outer disks. This is of no consequence provided the difference be known. The difference was measured with a comparator to within $\pm 5 \times 10^{-5}$ cm. The difference was also measured by running the machine slowly without lubricant until an easily measurable difference in total rotation developed between the outer disks and the central disk. The result confirmed the comparator readings.

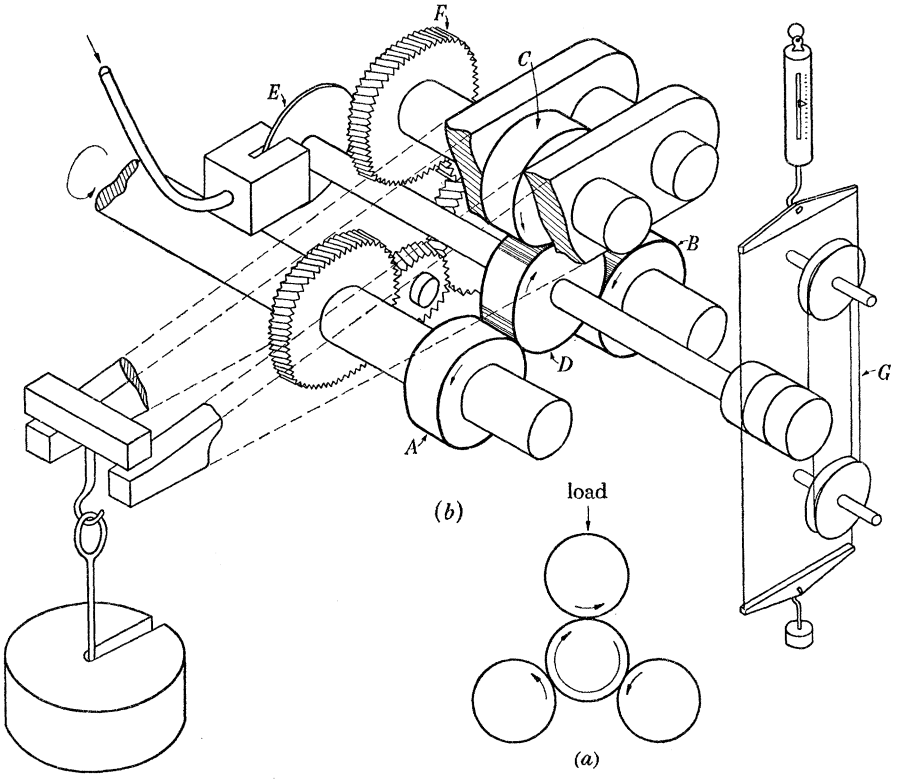

FIGURE 3. The four-disk machine. (*a*) Principle, (*b*) construction (diagrammatic). *A* to *D*, disks; *E*, aerostatic thrust; *F*, gear train; *G*, band brake.

So that small external torques can be applied to the central disk a band brake (*G*) is fitted. It consists of two ribbons of woven glass fibre each looped once round a 1 in. diameter steel cylinder and arranged so that they exert a pure torque. The combination of glass fibre and steel was advantageous in that it gave a steady friction free from fade despite temperatures which produced temper colours on the cylinder. The sliding of the disks was measured with a stroboscope lamp triggered from the driving shaft.

The machine is arranged with insulation to permit the measurement of the electrical capacitance between disks *C* and *D*. When measuring capacitance electrical connexion has to be made to the shaft of the central disk. This involves an unknown torque so capacitance measurements were made in separate experiments. For the measurement of surface temperature thermocouples as decribed in § 2 of part II (Crook 1961 *a*) are provided to bear upon disks *B* and *D*. The disks and gears of the machine were lubricated with oil to Admiralty specification OM 100. This oil has been described in part I (Crook 1958).

The machine is driven by a variable-speed motor with a maximum speed of 3000 rev/min.

(*b*) *Experimental*

The machine was run at the desired speed and load. The difference in rotational speed between the central disk and the outer disks was measured with the stroboscope. In further experiments the ribbons of the brake were fitted and the speed difference was measured for various values of the braking torque. In addition the surface temperature of the disks as given by the thermocouples was recorded.

In separate experiments the electrical capacitance between disks C and D was measured by the a.c. bridge method which has been described in part I.

(*c*) *Results*

The torque applied by the band brake was expressed as the frictional traction per unit face width (T_1) acting upon the central disk at each of its three conjunctions with the outer disks. The difference in rotational speed between the central disk and the outer disks was

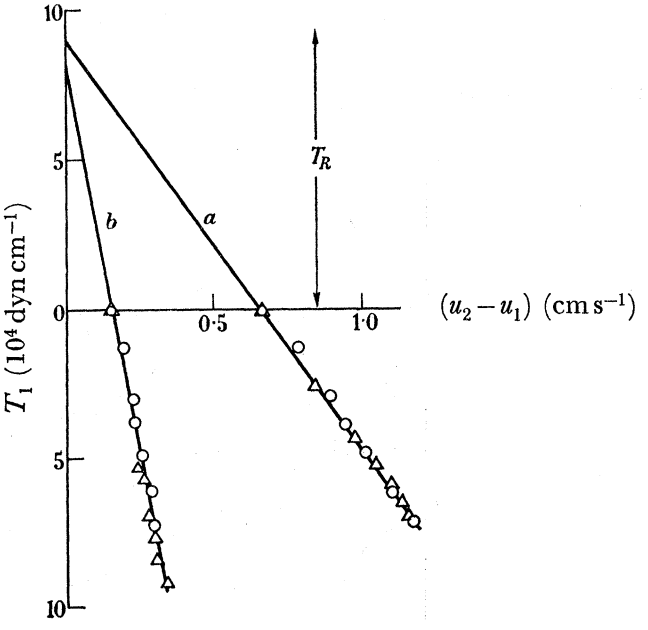

FIGURE 4. Surface traction (T_1) as a function of sliding speed (T_R is the rolling friction). (*a*) Load = $7{\cdot}4\times10^7$ dyn cm^{-1}, $\bar{u}=260$ cm s^{-1}, $\eta_s=0{\cdot}42$ P. (*b*) Load = 2×10^8 dyn cm^{-1}, $\bar{u}=300$ cm s^{-1}, $\eta_s=0{\cdot}4$ P. ○ and △ differentiate directions of rotation.

expressed as a sliding speed (u_2-u_1) allowance being made for the smaller diameter of the central disk. Typical plots of T_1 against (u_2-u_1) are given in figure 4. These show T_S (equation (2·4)) to be proportional to (u_2-u_1). The intercepts of the lines with the vertical axis give the values of T_R. Although the loads for the two sets of results given in figure 4 were very different, nevertheless, they both gave the same value for T_R.

From the values of surface temperature as recorded by the thermocouples and the known temperature dependence of the viscosity of the oil at atmospheric pressure (figure 3 of part I) a value of the viscosity at the surface temperature of a disk (η_s) was deduced for each of the disks B and D (figure 3). In general the two values differed slightly; the mean was used to evaluate $\bar{u}\eta_s$ where $\bar{u}$ is the rolling speed of the disks ($\bar{u}=\frac{1}{2}(u_1+u_2)$).

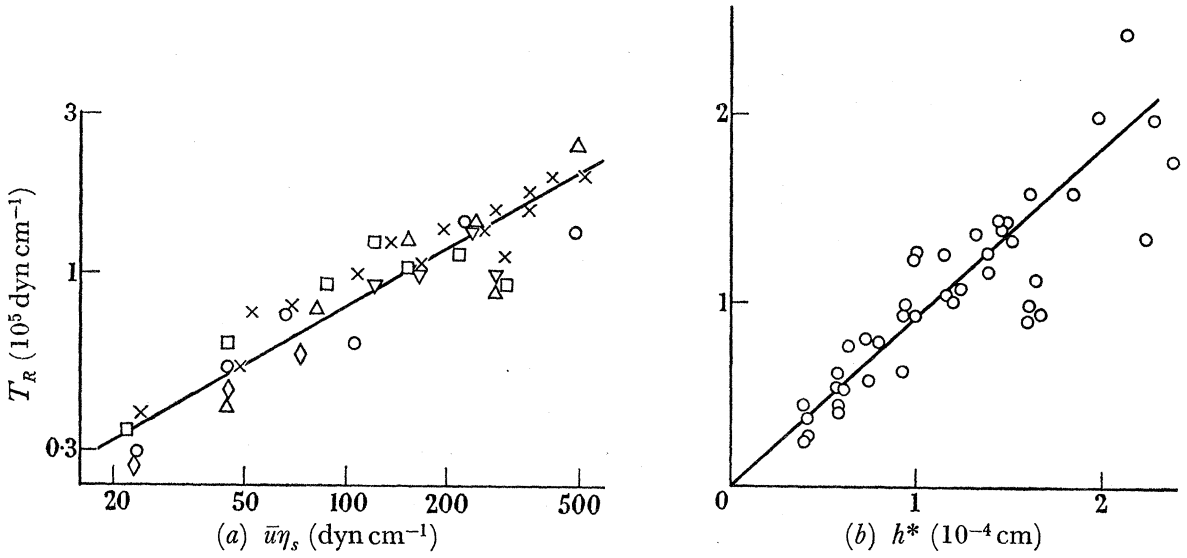

FIGURE 5. Rolling friction in relation to $\bar{u}\eta_s$ and film thickness (*a*) T_R as a function of $\bar{u}\eta_s$. Load (10^7 dyn cm^{-1}), ◇ 2·5, ○ 4·9, × 7·4, □ 10·0, △ 14·6, ▽ 19·7. (2×10^8 dyn cm^{-1} = 1120 Lb. in.$^{-1}$); (*b*) T_R as a function of film thickness (same results as for (*a*)).

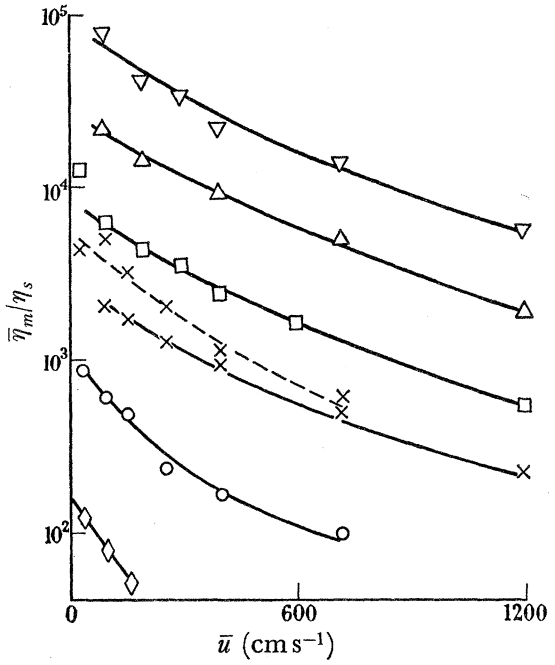

FIGURE 6. The ratio of the effective viscosity ($\bar{\eta}_m$) to η_s in pure rolling. Load (10^7 dyn cm^{-1}): ◇ 2·5, ○ 4·9, × 7·4, □ 10·0, △ 14·6, ▽ 19·7; —— 0·2 P < η_s < 0·6 P; ----- 0·6 P < η_s < 1·5 P (1000 cm s^{-1} = 1980 ft. min^{-1}).

It was found that a strong correlation exists between T_R and $\bar{u}\eta_s$ (figure 5 *a*). The figure embraces loads from $2{\cdot}5 \times 10^7$ dyn cm^{-1} to $1{\cdot}97 \times 10^8$ dyn cm^{-1}, values of $\bar{u}$ from 37 to 1200 cm s^{-1} and values of η_s from 0·24 P to 1·69 P and shows that for the range of loads explored no dependence of T_R upon load is discernible. (Because of this independence, in the context of the hydrodynamic lubrication of rollers, the concept of a coefficient of rolling friction is not useful; curve (*a*) of figure 4 gives a coefficient of $1{\cdot}4 \times 10^{-3}$ while curve

(b) gives a coefficient of 5×10^{-4}.) In addition figure 5 (a) shows that T_R is proportional to $(\bar{u}\eta_s)^{0\cdot5}$.

It is shown in appendix A that the film thicknesses (h^*) associated with the three conjunctions of the four disk machine are the same as those associated with the single conjunction of the two disk machine of parts I and II; in particular it is shown that $h^*\propto(u\eta_s)^{0\cdot5}$. It follows therefore that the rolling friction is simply proportional to the film thickness (figure 5 (b)).

The slopes of lines such as those of figure 4 were multiplied by their associated values of $h^*/2b$ (equation (4·9) below) where $2b$ is the width of the Hertzian flat. The products are the effective viscosities of the oil within the pressure zone ($\bar{\eta}_m$) and values of the ratio ($\bar{\eta}_m/\eta_s$) are plotted against $\bar{u}$ in figure 6. The effective viscosity increases with load but at constant load it falls as $\bar{u}$ increases.

4. Discussion

(a) *The rolling component of the friction*

From equation (2·4)

$$T_R=-\frac{1}{2}\int_{-2b}^{\infty}h\frac{\partial P}{\partial x}\,\mathrm{d}x=-\frac{1}{2}\left[(hP)_{x=\infty}-(hP)_{x=0}-\int_0^{\infty}P\frac{\partial h}{\partial x}\,\mathrm{d}x+\int_{-2b}^{0}h\frac{\partial P}{\partial x}\right]\mathrm{d}x.$$

If P be zero at $x=\infty$, $-2b$ and h be constant over the interval $0\geqslant x\geqslant-2b$ (i.e. $h=h^*$) it then follows that

$$T_R=\frac{1}{2}\int_0^{\infty}P\frac{\partial h}{\partial x}\,\mathrm{d}x. \tag{4·1}$$

Grubin (1949) has shown that if the viscosity of the oil varies with pressure according to

$$\eta_P=\eta_0\exp(\delta P),$$

then the pressure (P) is given by

$$P=-\frac{1}{\delta}\ln(1-\delta P'),\quad P'=12\bar{u}\eta_0\int_x^{\infty}\left(\frac{h-h^*}{h^3}\right)\mathrm{d}x. \tag{4·2}$$

(A fuller discussion of equation (4·2) has already been given in part II.)

At the entry edge of the Hertzian flat ($x=0$) P' may be set at a fraction of $1/\delta$ (§ 4 of part II). It will be set at κ/δ. It then follows from equation (4·2) that

$$P=-\frac{1}{\delta}\ln\left[\frac{(1-\kappa)\int_0^{\infty}\left(\frac{h-h^*}{h^3}\right)\mathrm{d}x+\kappa\int_0^{x}\left(\frac{h-h^*}{h^3}\right)\mathrm{d}x}{\int_0^{\infty}\left(\frac{h-h^*}{h^3}\right)\mathrm{d}x}\right]. \tag{4·3}$$

Approximately (equation (4·8) of part II)

$$h-h^*=h^*\chi^{\frac{3}{2}},\quad \chi=2b^{\frac{1}{3}}x/(3Rh^*)^{\frac{2}{3}}, \tag{4·4}$$

where b is the half width of the Hertzian flat and R is the relative radius of curvature of the disks. By use of equation (4·4) P can be expressed in terms of χ, i.e.

$$P=\frac{1}{\delta}f(\chi)=-\frac{1}{\delta}\ln\left[\frac{(1-\kappa)\int_0^{\infty}\Omega\,\mathrm{d}\chi+\kappa\int_0^{\chi}\Omega\,\mathrm{d}\chi}{\int_0^{\infty}\Omega\,\mathrm{d}\chi}\right],\quad \Omega=\frac{\chi^{\frac{3}{2}}}{(1+\chi^{\frac{3}{2}})^3}. \tag{4·5}$$

PHILOSOPHICAL TRANSACTIONS OF THE ROYAL SOCIETY A MATHEMATICAL, PHYSICAL & ENGINEERING SCIENCES

Also, from equation (4·4),

$$\frac{\partial h}{\partial x} = \tfrac{3}{2}h^*\chi^{\frac{1}{2}}\frac{\partial \chi}{\partial x}. \tag{4·6}$$

So, from equations (4·1), (4·5) and (4·6)

$$T_R \simeq \frac{3}{4}\frac{h^*}{\delta}\int_0^\infty \chi^{\frac{1}{2}} f(\chi)\,\mathrm{d}\chi = \alpha h^*. \tag{4·7}$$

This approximate theory shows that the rolling component of the friction should be proportional to film thickness, independent of load and also, except in so far as they bear upon film thickness, independent of the relative radius of curvature of the disks and of the elastic constants of the materials from which the disks are made. Proportionality with film thickness and independence of load have been demonstrated experimentally (figure 5 (*b*)).

The integral of equation (4·7) was evaluated numerically for values of κ from 0·7 to 1·0. (The numerical integration was carried up to $\chi = 6$. Over the interval $6 \leqslant \chi < \infty$ the integral was evaluated analytically from an approximate expression based upon $h = x^2/2R$ and valid for values of x large compared with b.) The corresponding values of α (equation (4·7)) were calculated assuming δ to be $2\times10^{-9}\,\mathrm{dyn^{-1}\,cm^2}$ and the values thereby obtained are given in table 1. In addition, in one instance, by assuming definite values for h^*, b and R (respectively 1×10^{-4} cm, 2×10^{-2} cm, 1·9 cm) T_R was evaluated from an expression for $(h-h^*)$ given by a more exact expression for the Hertzian shape. It was evaluated from

$$h-h^* = -\frac{b^2}{2R}[(1+\phi)\sqrt{(\phi^2+2\phi)} - \ln\{1+\phi+\sqrt{(\phi^2+2\phi)}\}], \quad \phi = x/b. \tag{4·8}$$

The value of α thereby obtained agrees closely with that obtained from equation (4·7) (table 1).

TABLE 1. VALUES OF α ($T_R = \alpha h^*$)

basis of evaluation of α	κ	$P_{x=0}$ ($10^9\,\mathrm{dyn\,cm^{-2}}$)	α ($\mathrm{dyn\,cm^{-2}}$)
by calculation from approximate Hertz shape (equation (4·7))	1·0	∞	13·5
	0·99	2·3	13·2
	0·9	1·2	11·2
	0·7	0·6	8·1
by calculation from exact Hertz shape (equation (4·8))	1·0	∞	13·6
experimental (figure 5 (*b*))	—	—	$\simeq 9$

The table shows that within 50 % the calculated values of α agree with the value obtained experimentally. It is evident that by assuming a sufficiently small value of κ exact agreement may be obtained, but by so doing the pressure attributed to the entry edge is depressed to too low a value. It would seem therefore that the calculated values are larger than the experimental value. The difference could be due to the approximate nature of the calculations or due to a systematic error in the measurement of film thickness. Nevertheless, within these limitations, the agreement is satisfactory. The agreement is particularly satisfactory in that both theory and experiment show T_R to be proportional to film thickness over a range of $\bar{u}\eta_s$ from 20 to 600 $\mathrm{dyn\,cm^{-1}}$. This provides further confirmation that in pure rolling the temperatures due to the friction are too small to affect the viscosity significantly (§ 4 of part III).

(b) The effective viscosity in pure rolling

The sliding component of the friction (T_S) is given by equation (2·4),

$$T_S = (u_2-u_1)\int_{-2b}^{\infty}\frac{\eta_m}{h}\,dx = (u_2-u_1)\int_0^{\infty}\frac{\eta_m}{h}\,dx+(u_2-u_1)\int_{-2b}^{0}\frac{\eta_m}{h}\,dx.$$

It may be shown that over the interval $\infty > x \geqslant 0$ the contribution to T_S is at most 10 %. Consequently the first integral on the right will be dropped. Then if $\bar{\eta}_m$ is the average value of η_m and h^* is the thickness of the parallel section of the film extending over the Hertzian width $2b$ it follows that

$$T_S \simeq 2\bar{\eta}_m(u_2-u_1)\,b/h^*. \tag{4·9}$$

The experimental results (figure 4), in keeping with equation (4·9), show T_S to be proportional to (u_2-u_1). Therefore over the range of speeds of sliding under consideration (up to a few cm s^{-1}) $\bar{\eta}_m$ is independent of (u_2-u_1). This implies that at such speeds of sliding the increments of temperature associated with the frictions are too low to have an appreciable effect upon the viscosity of the oil. The effect upon viscosity is estimated in appendix B and is found to be less than 1 %. Consequently the values of $\bar{\eta}_m$ deduced from the slopes of the experimental curves (figure 4) and equation (4·9) are valid at the rolling point although the experimental measurements themselves start at an appreciable speed of sliding.

(i) *The effect of pressure*

To remove the direct effect of variations in the viscosity of the oil at the surface temperature of the disks (η_s) the values of $\bar{\eta}_m$ deduced from the experimental results are presented as the ratio of $\bar{\eta}_m/\eta_s$ in figure 6. The figure shows that $\bar{\eta}_m/\eta_s$ rises with load (a thousand-fold increase on raising the load from $2{\cdot}5\times10^7$ to $19{\cdot}7\times10^7$ dyn cm^{-1}), falls with rolling speed (a 10-fold drop on increasing $\bar{u}$ from some tens to 1200 cm s^{-1}) and, for constant load and $\bar{u}$, rises perceptibly when η_s is increased (cf. the chain and continuous lines for a load of $7{\cdot}4\times10^7$ dyn cm^{-1}).

On passing through the conjunction the oil is compressed and becomes heated in consequence. This will have influenced the values of $\bar{\eta}_m/\eta_s$ given above but the effect is so small that it may be neglected (appendix C).

If viscosity increases exponentially with pressure in accordance with

$$\eta_P = \eta_0 \exp(\delta P)$$

and if the pressure distribution were Hertzian with a maximum pressure $P_{\text{max.}}$ then

$$\bar{\eta}_m/\eta_s = \frac{1}{b}\int_0^b \exp\{\delta P_{\text{max.}}\sqrt{(b^2-x^2)}/b\}\,dx; \tag{4·10}$$

from this $\bar{\eta}_m/\eta_s$ was calculated as a function of $\delta P_{\text{max.}}$ (figure 7) and values of δ corresponding to the values of $\bar{\eta}_m/\eta_s$ given in figure 6 were deduced. A representative selection of the values of δ so obtained are presented as a function of $\bar{u}$ in figure 8.

The actual pressure distribution is, of course, not exactly Hertzian as assumed in the derivation of equation (4·10). However, the departures occur mainly at entry where the pressures are low. The regions of low pressure contribute little to the integral of equation (4·10) in comparison with the region of high pressure. Consequently, although the actual

PHILOSOPHICAL TRANSACTIONS OF THE ROYAL SOCIETY A MATHEMATICAL, PHYSICAL & ENGINEERING SCIENCES

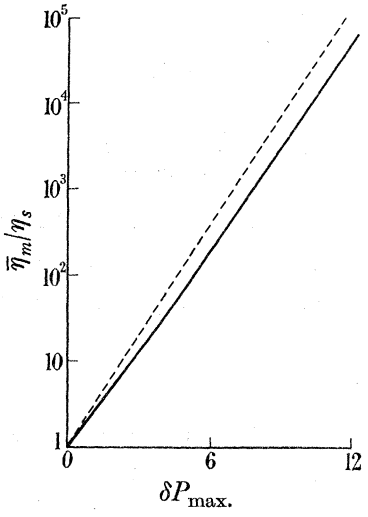

FIGURE 7

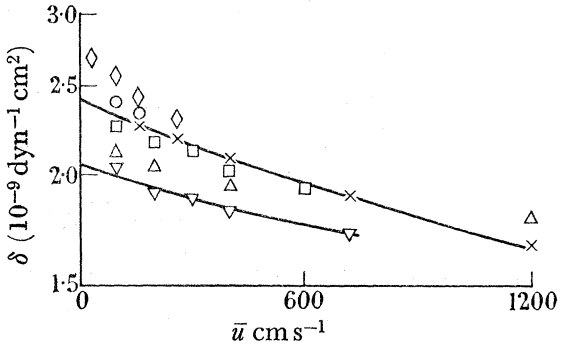

FIGURE 8

FIGURE 7. $\bar{\eta}_m/\eta_s$ as a function of $\delta P_{\max.}$ for isothermal conditions. ——, $\bar{\eta}_m/\eta_s$; – – – –, exp ($\delta P_{\max.}$).

FIGURE 8. The variation of δ with rolling speed. 0·35 P $< \eta_s <$ 0·45 P; load (10^7 dyn cm^{-1}): ○ 4·9, × 7·4, □ 10·0, △ 14·6, ▽ 19·7. 1·1 P $< \eta_s <$ 1·43 P; load (10^7 dyn cm^{-1}): ◇ 7·4.

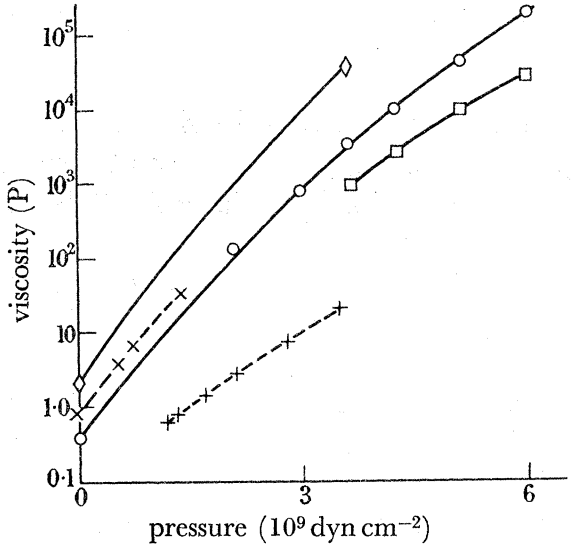

FIGURE 9. Viscosity as a function of pressure. —○—, $\bar{u} = 0$, 50 °C; —□—, $\bar{u} = 400$ cm s^{-1}, 50 °C; —◇—, $\bar{u} = 0$, 27 °C. – – – –, *Pressure Viscosity Report* 1953 (oil 29 F); ×, 38 °C, +, 99 °C. (1×10^9 dyn cm^{-2} ≃ 15 000 Lb. in.$^{-2}$.)

pressure distribution departs in detail from the Hertzian distribution, nevertheless, equation (4·10) is adequate.

The values of δ given in figure 8 show that δ falls as the load is increased, that δ rises as η_s is increased (i.e. as the surface temperature of the disks falls) and that δ falls as the rolling speed increases.

The variation of viscosity with pressure implied by these values of δ was calculated and the results are presented in figure 9. (The curve for $\bar{u} = 0$ was obtained by extrapolating lines such as the two drawn in figure 8 to $\bar{u} = 0$ and by calculating with the values of δ thereby found.) The figure also contains results from the *Pressure Viscosity Report* (1953) for

the oil of greatest similarity to the O M 100 oil of the present work. The *Pressure Viscosity Report* gives viscosity as a function of pressure as measured by a dropping ball type of viscometer in a high pressure apparatus following Bridgman (1949). The viscosities of the *Report* for the relevant oil do not extend beyond 40 P but in so far as that limit permits a comparison of the results of the *Report* with the viscosities as measured in the disk machine ($\bar{u} = 0$) shows the two sets of results to be in accord.

The fall in δ as the load increases (figure 8) and the decreasing slopes of the lines of figure 9 as the pressure rises are both a reflexion of the same behaviour. Such a decrease is a general feature of the curves of the *Pressure Viscosity Report*. In addition figure 8 shows that as the initial viscosity is increased (η_s increased) the rise of viscosity with pressure becomes more steep. Again this is a general feature of the *Pressure Viscosity Report*.

However, the results from the disk machine reveal a behaviour which could not be found with the sustained stress imposed by a dropping ball viscometer; they show that the variation of viscosity with pressure is also a function of rolling speed or, perhaps more generally, a function of the time for which the oil is under stress. The increase in viscosity with pressure becomes less as that time decreases.

(ii) *The effect of temperature*

Near the rolling point the temperature of the oil throughout the conjunction is effectively that of the disks themselves as the rise in temperature within the oil is small (appendices B and C). Therefore a change in $\bar{\eta}_m$, due to a change in disk temperature, exhibits the temperature dependence of the oil under the conditions of pressure and transit time pertaining to the conjunction.

It was assumed that the temperature dependence is of the form

$$(\bar{\eta}_m)_{\theta_2} = (\bar{\eta}_m)_{\theta_1} \exp\{-\gamma(\theta_2 - \theta_1)\},$$

where θ_1, θ_2 were identified with the disk temperatures. In figure 10 values of γ obtained in that way from pairs of results in which θ_2 and θ_1 differed by approximately 15 deg C are plotted against rolling speed ($\bar{u}$).

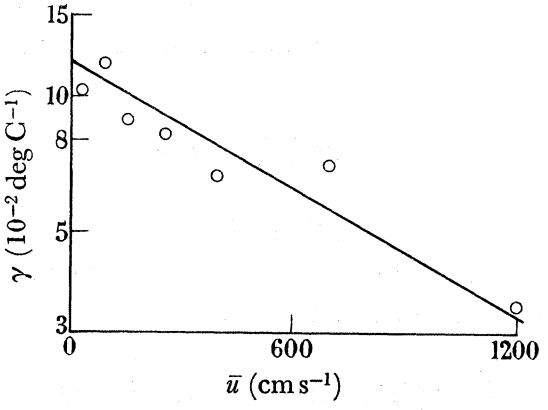

FIGURE 10. The variation of γ with rolling speed. (Load = $7{\cdot}4 \times 10^7$ dyn cm^{-1}.)

The figure shows that, like δ, the temperature coefficient γ also falls as $\bar{u}$ increases.

It may reasonably be supposed that at low rolling speeds the temperature dependence so determined should approach that determined more conventionally in a high-pressure apparatus.

In figure 11 results taken from the *Pressure Viscosity Report* (1953) for the oil most similar to the O M 100 of the disk experiments (oil 29 F of the *Report*) are given. To cover the viscosities of interest an extrapolation on the basis of the *A.S.T.M. Standard Viscosity-Temperature Chart* (1939) was made.

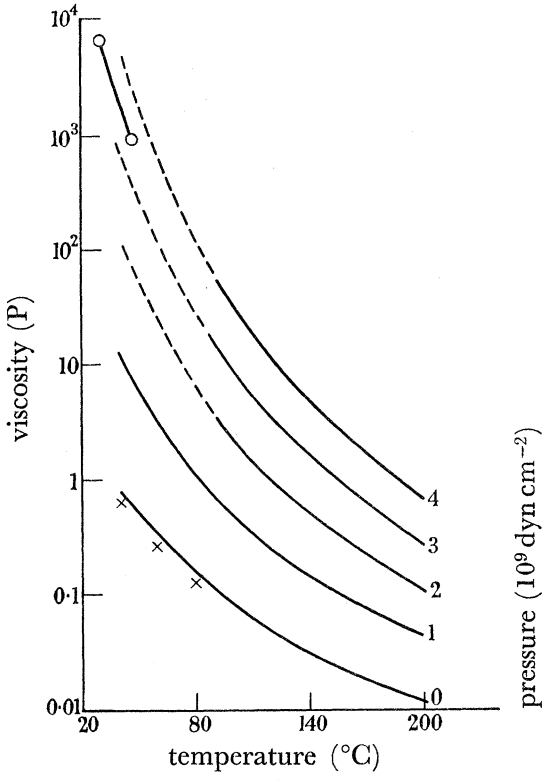

FIGURE 11. Viscosity as a function of temperature. Oil 29 F (*Pressure Viscosity Report* 1953). ——, Experimental; – – – –, extrapolated; ×, OM 100 at atmospheric pressure; ○, OM 100 from disk experiments, $\bar{u} = 100\,\mathrm{cm\,s^{-1}}$.

The disk experiments were conducted at a load of $7{\cdot}4 \times 10^7\,\mathrm{dyn\,cm^{-1}}$ which gives a maximum pressure of $3{\cdot}7 \times 10^9\,\mathrm{dyn\,cm^{-2}}$ and a representative pressure (P_r) of $3{\cdot}3 \times 10^9$ dyn cm^{-2}. (P_r is defined by

$$\exp \delta P_r = \frac{1}{b} \int_0^b \exp\{\delta P_{\max.} \sqrt{(b^2 - x^2)}/b\}\,\mathrm{d}x.)$$

The circular points in figure 11 give values of $\bar{\eta}_m$ obtained at a low speed of rolling and, in point of viscosity and rate of change of viscosity with temperature, agree with the expected behaviour of oil 29 F at a pressure equal to the representative pressure of the disk experiments.

(*c*) *Effective viscosity and rolling speed*

The explanation of the variation of viscosity with rolling speed must be also the explanation of why the slopes of plots such as those of figure 4 vary when rolling speed alone is changed. Rolling friction is the explanation of the varying intercepts; a viscosity varying with shear rate is a possible explanation of any curvature but to explain the varying slopes an effect dependent upon the time of transit has to be invoked. Visco-elasticity is such an effect.

For a visco-elastic fluid

$$\frac{\partial u}{\partial y} = \frac{\tau}{\eta_1} + \frac{1}{G}\frac{\partial \tau}{\partial x}u \quad \text{(Milne 1957; Crouch \& Cameron 1960),}$$

where in the co-ordinates of figure 12 u is velocity taken positive in the negative direction of x, τ is shear stress and G is the elastic modulus of the fluid in shear.

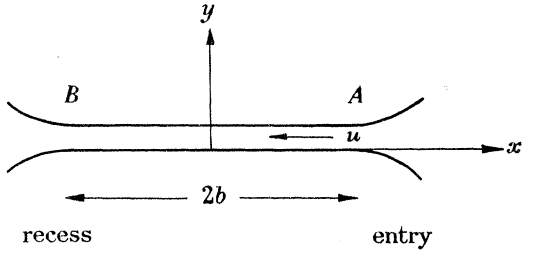

FIGURE 12. Co-ordinates for visco-elastic hypothesis.

It will be assumed that the fluid enters at A (figure 12) free from elastic strain and that the pressure is constant from A to B. Constant pressure implies that τ is independent of y (Milne 1957) when integration of the above expression gives

$$\frac{\eta_2}{\eta_1} = 1 - \frac{\lambda}{t}\left[1 - \exp\left(-\frac{t}{\lambda}\right)\right], \tag{4·11}$$

where η_2 is the apparent viscosity defined by

$$\eta_2 = h^* \int_{-2b}^{0} [\tau/(u_2 - u_1)]\, dx,$$

where λ is the relaxation time of the fluid defined by

$$\lambda = \eta_1/G$$

and where t is the mean time for which the fluid is subjected to stress and is defined by

$$t = 4b/(u_1 + u_2).$$

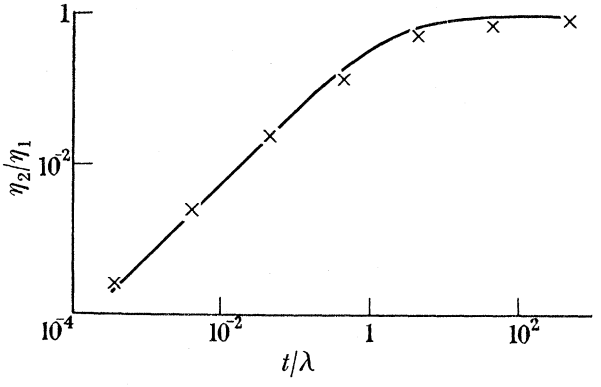

FIGURE 13. The ratio of the apparent viscosity (η_2) to the actual viscosity (η_1) as a function of t/λ. ——, Equation (4·11); ×, Crouch & Cameron (1960).

In figure 13 η_2/η_1 as deduced from the theory of Crouch & Cameron (1960) (in which a parabolic distribution of pressure was assumed and a viscosity rising exponentially with pressure) and also as calculated from equation (4·11) is plotted. The two sets are close so the precise form of the pressure distribution is of little importance.

For each curve of figure 6 the values of $\bar{\eta}_m$ at rolling speeds of 600 and 1200 cm s^{-1} were expressed as ratios of $\bar{\eta}_m$ at zero rolling speed. These ratios were identified with η_2/η_1 of equation (4·11) and from figure 13 values of λ/t and hence of G were deduced (figure 14). (At 1200 cm s^{-1} the values of G were approximately 50 % greater than those for 600 cm s^{-1}. The means are plotted in the figure.) The points fall on a smooth curve. In addition the variation of $\bar{\eta}_m/\eta_s$ with rolling speed implied by the values of G were calculated. The calculated curves together with the experimental points are given in figure 15.

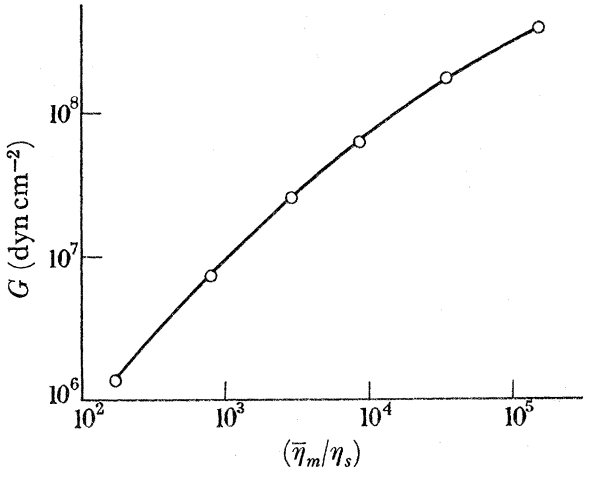

FIGURE 14

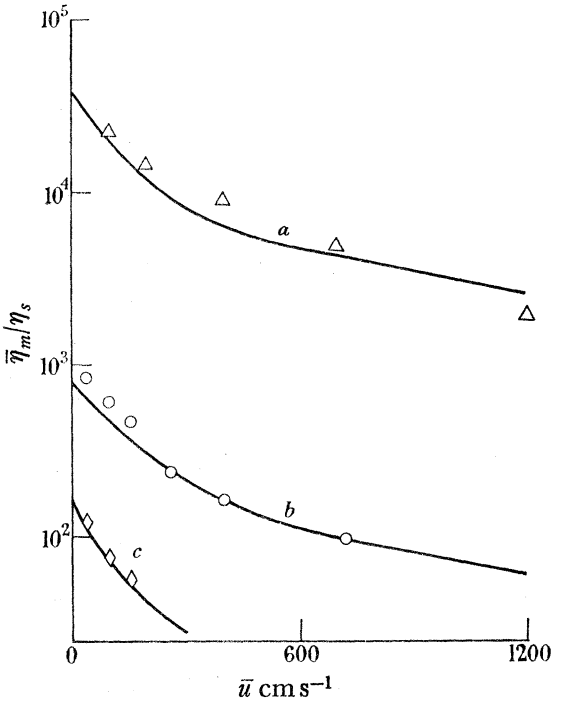

FIGURE 15

FIGURE 14. Shear modulus (G) as a function of $(\bar{\eta}_m/\eta_s)$ at zero rolling speed.

FIGURE 15. The ratio of the effective viscosity $(\bar{\eta}_m)$ to η_s in pure rolling. ——, Calculated from the visco-elastic hypothesis (*a*) $G = 1{\cdot}9 \times 10^8$ dyn cm^{-2}; $\lambda = 1{\cdot}9 \times 10^{-4}$ s; (*b*) $G = 7{\cdot}4 \times 10^6$ dyn cm^{-2}, $\lambda = 1{\cdot}1 \times 10^{-4}$ s; $G = 1{\cdot}4 \times 10^6$ dyn cm^{-2}, $\lambda = 1{\cdot}2 \times 10^{-4}$ s. Experimental points, load (10^7 dyn cm^{-1}): ◇ 2·5, ○ 4·9, △ 14·6.

The variation of the temperature dependence of viscosity with respect to rolling speed (figure 10) can also be described in terms of visco-elasticity. Experimental values of $\bar{\eta}_m$ for a load of $7{\cdot}4 \times 10^7$ dyn cm^{-1} and for temperatures of approximately 30 and 45 °C were adjusted to those temperatures assuming an exponential dependence (figure 16).

In column (i) of table 2 values of $\bar{\eta}_m$ at $\bar{u} = 0$ are entered and in column (iii) the ratios $\bar{\eta}_m/\eta_s$ for $\bar{u} = 0$ are given. The values of G implied by these ratios were obtained from figure 14 and are given in column (iv) with the relaxation time (λ) in column (v). The ratio t/λ for $\bar{u} = 400$ cm s^{-1} is given in column (vi) where t is the time of transit through the Hertzian width $2b$. The values of η_2/η_1 (column (vii)) associated with the values of t/λ were obtained from figure 13 and by identifying η_1 with the value of $\bar{\eta}_m$ at $\bar{u} = 0$ values of η_2 were calculated (column (viii)). In that way the variation of the apparent viscosity (η_2) with rolling speed

as predicted by the visco-elastic hypothesis was calculated (interrupted lines of figure 16). There is a qualitative agreement in that the calculated curves also indicate that the apparent viscosity becomes less sensitive to a change in temperature as the rolling speed increases.

Thus with appropriate values of G the visco-elastic hypothesis can be made to account qualitatively for the observations; it does predict sensitivities of viscosity to changes in both pressure and temperature which decrease with the transit time.

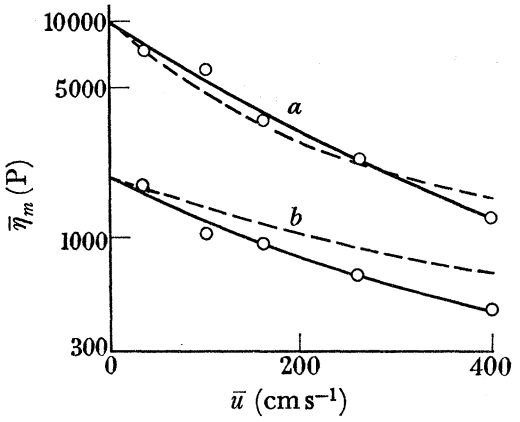

FIGURE 16. The effective viscosity ($\bar{\eta}_m$) as a function of rolling speed. (*a*) 30 °C; (*b*) 45 °C. —○— deduced from experimental results; – – – –, calculated from visco-elastic hypothesis. Load = $7{\cdot}4 \times 10^7$ dyn cm^{-1}.

TABLE 2. VISCO-ELASTICITY AND THE TEMPERATURE DEPENDENCE OF VISCOSITY

θ_s (°C)	$\bar{\eta}_m$ ($\bar{u}=0$) P (i)	η_s P (ii)	$\bar{\eta}_m/\eta_s$ ($\bar{u}=0$) (iii)	G (dyn cm^{-2}) (iv)	$\lambda=\bar{\eta}_m/G$ ($\bar{u}=0$) s (v)	$t=2b/\bar{u}$ ($\bar{u}=400$ cm s^{-1}) s	t/λ (vi)	η_2/η_1 (vii)	η_2 P (viii)
45	$2{\cdot}0 \times 10^3$	0·49	$4{\cdot}1 \times 10^3$	$3{\cdot}3 \times 10^7$	$6{\cdot}0 \times 10^{-5}$	$6{\cdot}3 \times 10^{-5}$	1·05	0·38	$7{\cdot}6 \times 10^2$
30	$9{\cdot}5 \times 10^3$	1·20	$7{\cdot}9 \times 10^3$	$5{\cdot}6 \times 10^7$	$1{\cdot}7 \times 10^{-4}$	$6{\cdot}3 \times 10^{-5}$	0·37	0·16	$1{\cdot}52 \times 10^3$

The only other experimental evidence for visco-elastic effects in lubricants has been provided by measurements of shear waves generated in fluids by vibrating crystals (Mason, Baker, McSkimin & Heiss 1949; Barlow & Lamb 1959). Such measurements show a distribution of relaxation times and in particular times associated with a shear modulus of 1×10^7 dyn cm^{-2} termed 'configurational' elasticity and a modulus of the order 1×10^{10} dyn cm^{-2} termed 'crystalline' elasticity (Mason *et al.* 1949). The values of G postulated from the present experiments lie within the configurational régime.

With poly*iso*butylene Mason *et al.* (1949) found that within the 'configurational' régime G falls with viscosity when viscosity is varied by temperature or by the use of polymers of different mean molecular weights. From the present work G also falls with viscosity (figure 14). Against such similarities, however, must be set the fact that with lubricating oils of mineral origin Barlow & Lamb (1959) found that the elasticities were confined to the region of 1×10^{10} dyn cm^{-2}. But the conditions of the two sets of experiments are different both with respect to pressure (Barlow & Lamb worked chiefly at atmospheric pressure and in a few instances at a pressure of 1×10^9 dyn cm^{-2}) and with respect to the magnitude of the shear strains (the strains of the disk experiments are many orders of magnitude greater than those of the shear waves).

PHILOSOPHICAL TRANSACTIONS OF THE ROYAL SOCIETY A MATHEMATICAL, PHYSICAL & ENGINEERING SCIENCES

(*d*) *Effective viscosity and film thickness*

With δ constant theory gives a film thickness proportional to $(\bar{u}\eta_s)$ raised to a power of approximately 0·7 (part II). In figure 17 the depression of the exponent due to the variation of δ with $\bar{u}$ as found for a load of $7{\cdot}4 \times 10^7$ dyn cm^{-1} is illustrated (η_s was taken constant at 0·5 P); with the variation taken into account an exponent markedly closer to the experimental value of 0·5 is given. Furthermore, as film thickness is determined in the entry zone (part II) where the representative pressures and transit times will be less than those associated with $\bar{\eta}_m$, a more severe depression of δ with rolling speed than that assumed in figure 17 might be appropriate with respect to film thickness.

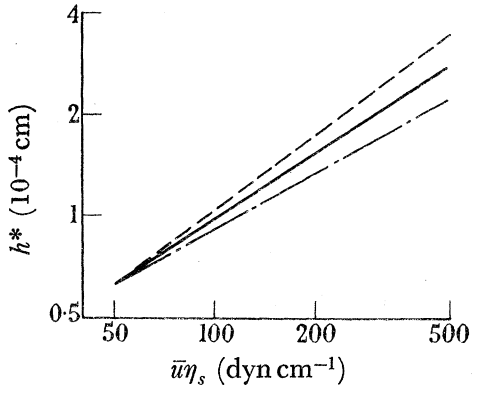

FIGURE 17. Film thickness as a function of $\bar{u}\eta_s$. ———, From equation (4·9) of part II, δ constant; ——, δ decreasing as $\bar{u}$ increases; —·—, experimental (figure 3 (*a*) of part II).

5. MEASUREMENTS AT SPEEDS OF SLIDING UP TO 400 CMS^{-1}

(*a*) *Apparatus*

As the sliding speed increases the friction rises, reaches a maximum and then falls. To explore the falling part of the curve of friction against sliding speed, controlled rotation of all the disks becomes necessary as on the falling part of the curve a brake brings its associated disk to rest (§ 10 of part III). Because of this and because of the large frictional forces to be measured it was convenient to adapt the two-disk machine (part I) for the work.

A diagram showing the principle of the machine is given in figure 18. The disk *A* (3 in. diameter) runs in bearings in the machine frame (not shown) and is driven by a variable speed motor. The disk *B* (3 in. diameter) runs in self-alining bearings in the swinging arms *C* and *D* which hang from the axle *E*. The rotation of the disk *B* is controlled through a cardan shaft by a variable speed motor which, in most instances, acted regeneratively. The disks are loaded together by equal tensions in the cables *F* and *G*. The friction at the conjunction of the disks is a vertical force. Vertical movement of the disk *B* and its associated swinging arms is controlled by the spring beam *H* to which the axle *E* is connected. The frictional force at the conjunction of the disks is transmitted to beam *H* and the change in its deflexion is measured by the dial gauge *I*. After calibration by dead loading the frictional force was obtained from appropriate readings of the dial gauge. The advantage of this system compared with conventional systems in which the friction is measured by dynamometers whose readings relate to the driving torques, is that the system gives measurements independent of friction in the bearings.

The axle E must be constrained so that is can only move vertically; the vertical movement of the axle with all its associated parts and dial gauge must be free from hysteresis and the cardan shaft controlling the rotation of disk B must not exert a vertical force, particularly a force which reverses upon change in the direction of rotation. Measures were taken to satisfy these requirements.

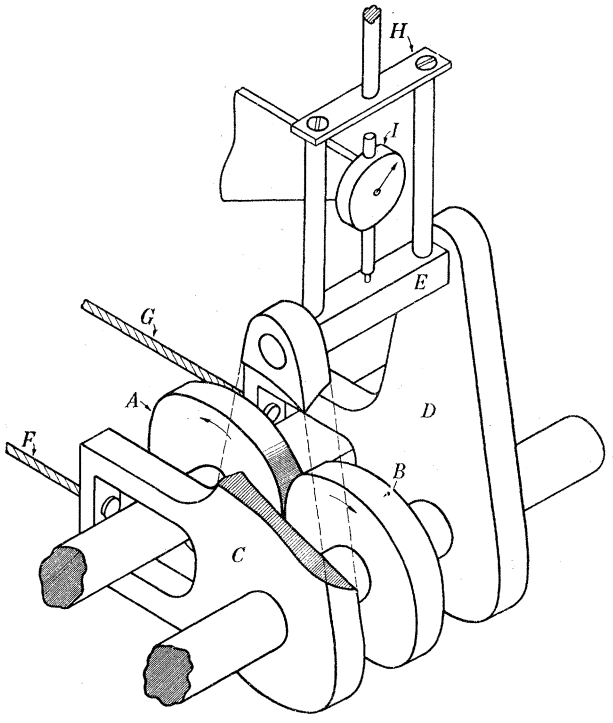

FIGURE 18. The two-disk machine arranged for the measurement of friction. A and B disks; C and D swinging arms; E axle; F and G loading cables; H spring beam; I dial gauge.

If the directions of the pulls exerted by the cables F and G are not parallel with the line of centres of the disks, then the reaction at the conjunction of the disks will have a vertical component. Unlike the friction this vertical component will not change direction on reversing the directions of rotation of the disks. The cables were carefully set to be parallel with the line of centres, but to eliminate any remaining vertical component the friction measurements were always taken in pairs; one measurement for each direction of rotation. But however accurate the initial setting of the cables that setting is disturbed as soon as the beam H deflects under the influence of the frictional force. With the vertical movement of disk B known correction can readily be made, but in general a beam H was chosen which was so stiff that no correction was necessary. However, with the beam so stiff the movement to be registered by the dial gauge became inconveniently small so a mechanical magnification of ten was interposed between the axle E and the dial gauge. The magnified movement was also employed to damp, by means of an oil-filled dash-pot, vibration of the axle E.

To measure the speeds of the disks triggers were arranged on both shafts to operate electronic counters. Counts over known intervals of time were taken. The capacitance bridge (part I) was used to measure the electrical capacitance between the two disks and a trailing thermocouple (part II) was used to measure surface temperature.

Upon analysis of the results it was seen that measurements of friction in close detail should be made from as near as possible to the rolling point up to sliding speeds of about 30 cm s^{-1}. Near the rolling point the frictional forces were inconveniently small for measurement with the two disk machine so the four disk machine was used. But above a few cm s^{-1} sliding the frictional forces were beyond the capability of the band brake of the four-disk machine (figure 3). The band brake of the four-disk machine was replaced by a dynamometer consisting of a 9 in. diameter disk brake. The dynamometer was floated in an aerostatic bearing. Electronic counters were used to measure speeds of rotation.

(*b*) *Experimental*

The two-disk machine was run so that in any series of experiments at a fixed load the sum of the speeds of the disks was held constant while the difference between the speeds of the two disks was varied. Friction, capacitance and disk temperature were measured. An attempt was also made to keep the temperature of the disks constant so as to minimize the variation of η_s over a series of measurements. This was done by runnning the machine at a light load until thermal equilibrium was reached before each measurement was made. The readings were taken as quickly as possible once the load was imposed and before frictional heating had raised the temperature of the disks seriously.

A similar procedure was used with the four-disk machine.

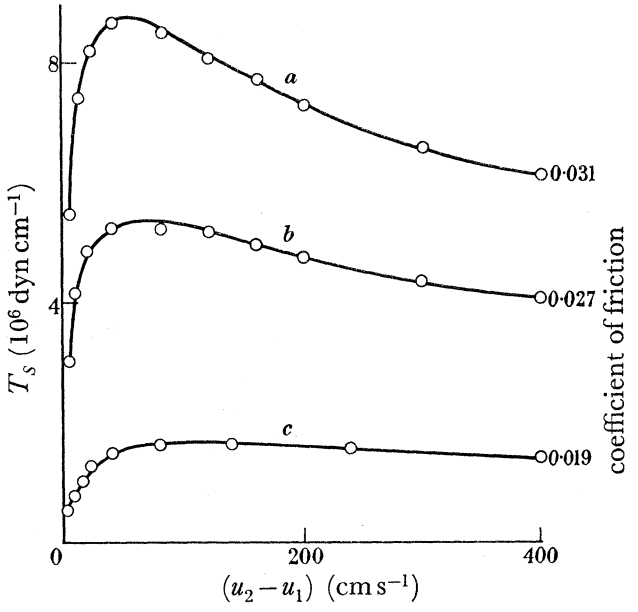

FIGURE 19. Frictional traction as a function of sliding speed; (rolling speed constant at 400 cm s^{-1}). Load (10^7 dyn cm^{-1}): (*a*) 20, (*b*) 15, (*c*) 7·5.

(*c*) *Results*

The frictional tractions were plotted against speed of sliding. Typical results for three loads (2×10^8, $1{\cdot}5 \times 10^8$ and $7{\cdot}5 \times 10^7$ dyn cm^{-1}) and for a rolling speed ($\bar{u}$) of 400 cm s^{-1} are given in figure 19. Over the curve for the lowest load (curve *c*) η_s varied from 0·43 P at low speeds of sliding down to 0·41 P at a sliding speed of 400 cm s^{-1}. At the highest load (curve *a*) the variation was greater because of the greater frictional heating; from 0·43 to 0·35 P.

In figure 20 all the results refer to the same load ($1{\cdot}25 \times 10^8$ dyn cm^{-1}) but $\bar{u}$ and η_s vary. Curves *a*, *b*, *c* and *e* all refer to an η_s nominally of 0·4 P but to values of $\bar{u}$ from 120 to 600 cm s^{-1}. Curve *d* is for an η_s nominally of 0·7 P and a $\bar{u}$ of 400 cm s^{-1}.

A typical result of the measurement in detail of friction up to a sliding speed of 30 cm s^{-1} is given in figure 21 (four-disk machine, disk brake). The curve is for a load of $1{\cdot}2 \times 10^8$ dyn cm^{-1}, a $\bar{u}$ of 400 cm s^{-1} and an η_s of 1·4 P.

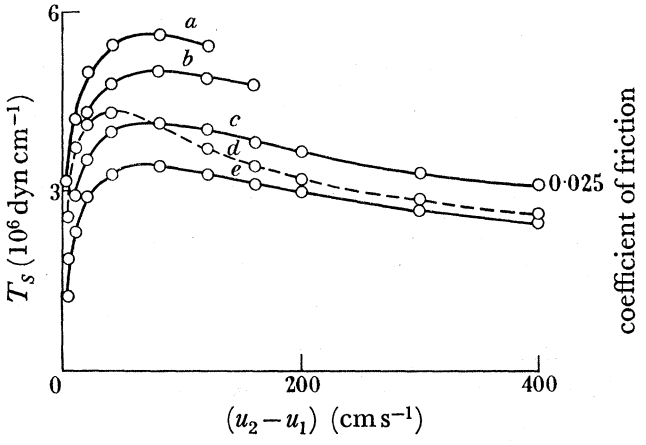

FIGURE 20. Frictional traction as a function of the speed of sliding. Load $1{\cdot}25 \times 10^8$ dyn cm^{-1}; (*a*) $\bar{u} = 120$ cm s^{-1}, $\eta_s \simeq 0{\cdot}4$ P; (*b*) $\bar{u} = 200$ cm s^{-1}, $\eta_s \simeq 0{\cdot}4$ P; (*c*) $\bar{u} = 400$ cm s^{-1}, $\eta_s \simeq 0{\cdot}4$ P; (*d*) $\bar{u} = 400$ cm s^{-1}, $\eta_s \simeq 0{\cdot}7$ P; (*e*) $\bar{u} = 600$ cm s^{-1}, $\eta_s \simeq 0{\cdot}4$ P.

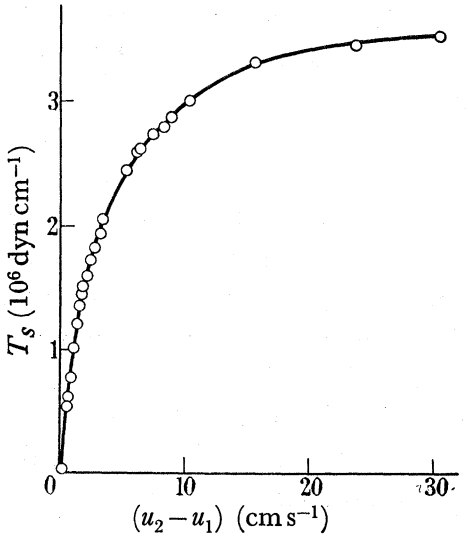

FIGURE 21. Frictional traction as a function of sliding speed (measurements in detail up to $u_2-u_1 = 30$ cm s^{-1}). Load $= 1{\cdot}2 \times 10^8$ dyn cm^{-1}, $\bar{u} = 400$ cm s^{-1}, $\eta_s \simeq 1{\cdot}4$ P.

6. COMPARISON WITH THEORY

(*a*) *Friction*

Salient features of figure 19 are that the frictional tractions increase as the load is increased, that at constant load the friction rises, reaches a maximum and then falls, that the sliding speed at which the maximum traction occurs increases as the load is reduced and that at a sliding speed of 400 cm s^{-1} the coefficient of friction increases as the load is increased.

These features are also exhibited by the theoretical frictional traction—sliding speed curves presented in part III (figure 12 of part III). Salient features of figure 20 are that at constant load, sliding speed and η_s the frictional traction falls as the rolling speed ($\bar{u}$) is increased, and that when η_s is increased the friction rises more rapidly with sliding speed, reaches it maximum at a smaller sliding speed and then falls more rapily so that ultimately the higher value of η_s gives the lower friction (cf. curves *c* and *d*). These features also are exhibited by the theory of friction of part III.

There are, therefore, a number of qualitative similarities between the experimentally determined values of friction and those calculated theoretically. Furthermore, the theory predicts coefficients of friction of the right order, e.g. a theoretical coefficient of 0·05 and an experimental coefficient of 0·03.

In calculating the theoretical curves values for the pressure coefficient of the oil (δ), its temperature coefficient (γ) and its thermal conductivity (K_0) were drawn from the available results of experiments in high-pressure apparatus following Bridgman. It is unlikely that these values will be accurate for the very different conditions of the disk experiments or, that in view of the variation of temperature which occurs within the film as the sliding speed is changed, that the actual values will be constant.

(*b*) *Effective viscosity*

Values of film thickness (h^*) were deduced from the measurements of the capacitance between the disks. From the frictional tractions values of the effective viscosity ($\bar{\eta}_m$) were then obtained (equation (4·9)). Typical results are given in figure 22 in which $\bar{\eta}_m$ is plotted against the speed of sliding. Upon the introduction of 400 cm s^{-1} sliding the curves show a fall in $\bar{\eta}_m$ of about two decades; the fall increased with load, e.g. a factor of 48 at a load of $7{\cdot}5\times10^7$ dyn cm^{-1} but a factor of 167 at a load of 2×10^8 dyn cm^{-1}. The curves of figure 22 (*b*) show that $\bar{\eta}_m$ is insensitive both to rolling speed and, at high values of (u_2-u_1), to η_s; the value of η_s associated with point *A* was 0·37 P and that associated with point *B* was 0·68 P which is a fractional increase of 0·8, whereas the associated fractional increase in $\bar{\eta}_m$ is only 0·25. These features are qualitatively in agreement with theory (part III) which predicts that $\bar{\eta}_m$ should be independent of rolling speed and that at high speeds of sliding a fractional change in $\bar{\eta}_m$ produced by a change in η_s should be small compared with the fractional change in η_s (equation (9·6) of part III).

In § 7 of part III a method of calculating $\bar{\eta}_m$ based upon the heat balance within the oil film has been described. In general the method requires numerical integration with respect to x of

$$\eta_m = \eta_x f(\psi),$$

where η_x is defined by $\quad \eta_x = \eta_s \exp(\delta P),$

where ψ is defined by $\quad \psi = \eta_x \gamma (u_2-u_1)^2/8K_0,$

and where $f(\psi)$ may be found from figure 9 of part III. However, it was also shown that at large values of (u_2-u_1) the approximation

$$\bar{\eta}_m = \frac{4K_0}{b\gamma(u_2-u_1)^2}\left[\tfrac{1}{2}\delta F + 2b\ln(u_2-u_1) + b\ln\left(\frac{\gamma\eta_s}{2K_0}\right)\right], \qquad (6{\cdot}1)$$

where F is the load per unit face width, is adequate (figure 11 of part III). From equation (6·1) it follows that

$$\frac{K_0}{\gamma} = \frac{(u_2-u_1)^3}{8}\left[\frac{2\bar{\eta}_m}{(u_2-u_1)} + \frac{\partial\bar{\eta}_m}{\partial(u_2-u_1)}\right], \tag{6·2}$$

in this δ does not appear.

Experimental values at a sliding speed of $350\,\mathrm{cm\,s^{-1}}$ were used to calculate K_0/γ from equation (6·2) and then δ from equation (6·1). By numerical integration $\bar{\eta}_m$ was calculated as a function of (u_2-u_1). It was found that small adjustments of the values of K_0/γ and of δ as found above produced a better agreement between the calculated and experimental curves (figure 22). The values of K_0/γ and of δ which were adopted together with the values of δ at $(u_2-u_1)=0$, $\bar{u}=400\,\mathrm{cm\,s^{-1}}$ as drawn from figure 8 are given in table 3.

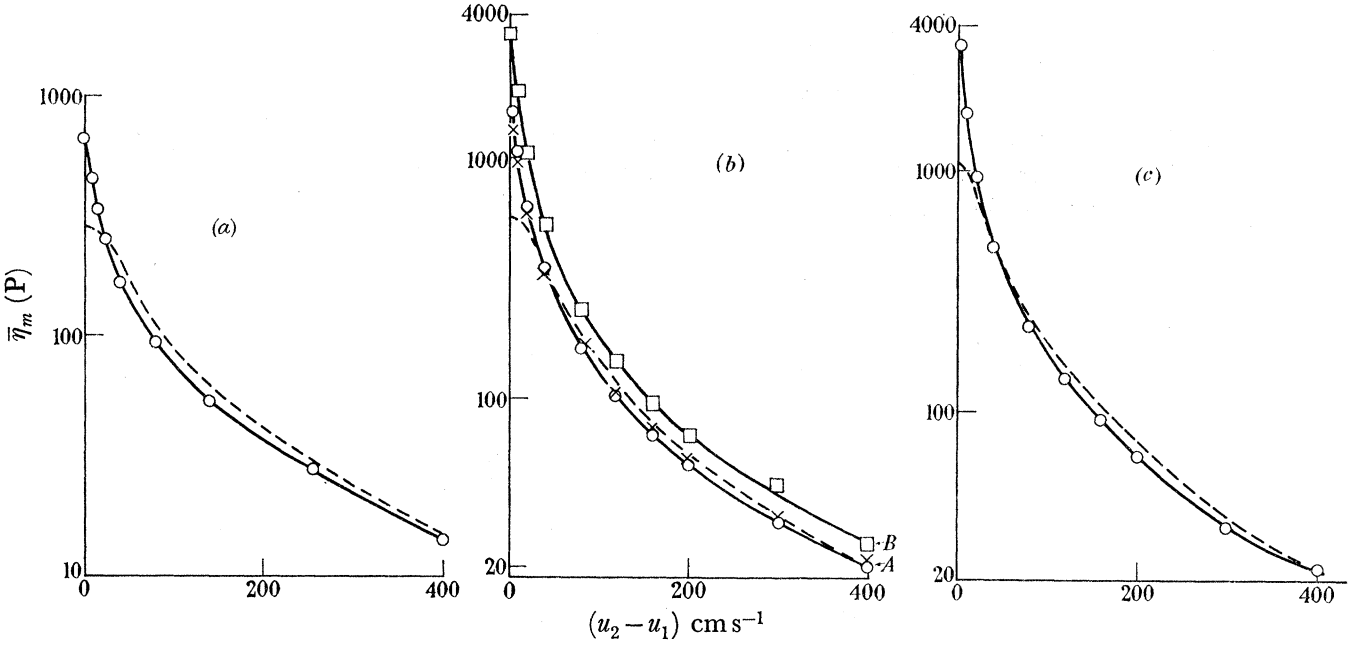

FIGURE 22. Effective viscosity as a function of sliding speed. (*a*) Load $= 7{\cdot}5\times10^7\,\mathrm{dyn\,cm^{-1}}$, $\bar{u}=400\,\mathrm{cm\,s^{-1}}$, $\eta_s\simeq 0{\cdot}4\,\mathrm{P}$, —○— experimental; ---- calculated. (*b*) Load $= 1{\cdot}25\times10^8\,\mathrm{dyn\,cm^{-1}}$. Experimental: ○, $\bar{u}=400\,\mathrm{cm\,s^{-1}}$, $\eta_s\simeq 0{\cdot}4\,\mathrm{P}$; ×, $\bar{u}=600\,\mathrm{cm\,s^{-1}}$, $\eta_s\simeq 0{\cdot}4\,\mathrm{P}$; □, $\bar{u}=400\,\mathrm{cm\,s^{-1}}$, $\eta_s\simeq 0{\cdot}7\,\mathrm{P}$. ----, Calculated for $\eta_s=0{\cdot}4\,\mathrm{P}$. (*c*) Load $= 2\times10^8\,\mathrm{dyn\,cm^{-1}}$, $\bar{u}=400\,\mathrm{cm\,s^{-1}}$, $\eta_s\simeq 0{\cdot}4\,\mathrm{P}$. —○—, Experimental; ----, calculated.

TABLE 3. VALUES OF K_0/γ AND OF δ

load ($\mathrm{dyn\,cm^{-1}}$)	$\bar{u}$ ($\mathrm{cm\,s^{-1}}$)	K_0/γ ($10^5\,\mathrm{dyn\,s^{-1}}$)	δ $(u_2-u_1)=350\,\mathrm{cm\,s^{-1}}$ ($10^{-9}\,\mathrm{dyn^{-1}\,cm^2}$)	δ $(u_2-u_1)=0$ ($10^{-9}\,\mathrm{dyn^{-1}\,cm^2}$)
$7{\cdot}52\times10^7$	400	1·3	1·95	2·1
$1{\cdot}25\times10^8$	400	1·7	1·67	1·9
$2{\cdot}0\times10^8$	400	1·8	1·43	1·8

(i) *The temperature at the surfaces of the disks*

The calculated curves of figure 22 were obtained without reference to the rise in temperature of the disks (θ_x) due to the flow of heat into them. The rise in temperature can be deduced from the frictional traction without reference to the properties of the oil (equation

(9·5) of part III) and values of θ_x for the conditions of curve (*c*) of figure 22 at 400 cm s^{-1} are given in figure 23.

It has been shown in part III that θ_x has little influence upon η_m so a change in θ_x implies new values of $f(\psi)$ (equation (7·4) of part III) and hence new values of K_0/γ (equation (5·9) of part III). In that way values of K_0/γ corrected for the influence of θ_x were obtained; for instance, a value of $1{\cdot}8 \times 10^5$ dyn s^{-1} obtained previously upon correction became $2{\cdot}4 \times 10^5$ dyn s^{-1}. The corrected values of η_m and of the temperatures on the medium plane of the oil film are shown together with the uncorrected values in figure 24. The differences are not large.

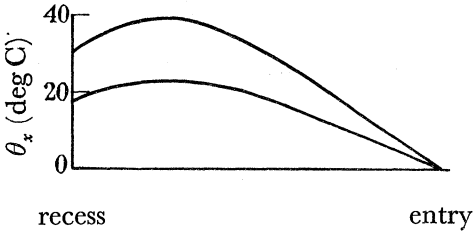

FIGURE 23. The rise in temperature at the surfaces of the disks. Load = 2×10^8 dyn cm^{-1}, $\bar{u} = 400$ cm s^{-1}, $(u_2 - u_1) = 400$ cm s^{-1}. Upper curve for surface with $u_1 = 200$ cm s^{-1}, lower for surface with $u_2 = 600$ cm s^{-1}.

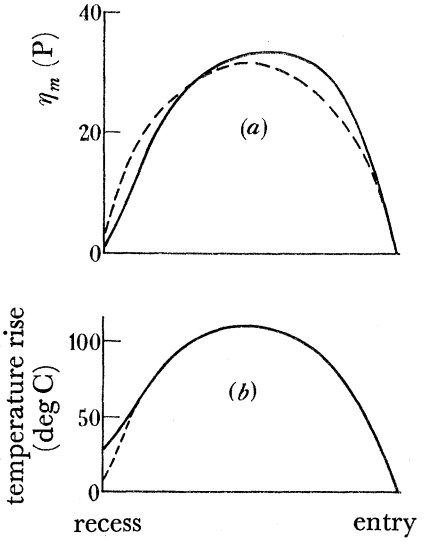

FIGURE 24. Conditions within the conjunction of the disks. Load = 2×10^8 dyn cm^{-1}, $\bar{u} = 400$ cm s^{-1}, $(u_2 - u_1) = 400$ cm s^{-1}. (*a*) η_m; (*b*) the temperature rise on the median plane of the film referred to the disk temperature at entry. – – –, $\theta_x = 0$; ——, variation in surface temperature taken into account.

(ii) *The values of K_0 and of γ*

Neglecting θ_x gives a viscosity at the surfaces of the disks (η_x) constant and equal to η_s. If θ_x had been regarded but γ had been set to zero again η_x equal to η_s would be given.

Within the film it is K_0/γ which alone is of importance. So the correction of K_0/γ already given can also be seen as arising from a change in γ from zero to the value assumed in calculating η_x; clearly K_0/γ is insensitive to the value of γ.

The value of γ is influenced by pressure and temperature (slopes of curves of figure 11) and by rolling speed (figure 16). By noting the temperature rise on the median plane given

by figure 24 (*b*) and also the pressure and rolling speed pertaining to the particular conditions, a value of γ of 5×10^{-2} deg C^{-1} was chosen. This value gives $1{\cdot}2\times10^{4}$ dyn s^{-1} deg C^{-1} as the value of $K_0(K_0/\gamma = 2{\cdot}4\times10^{5}$ dyn s$^{-1})$.

This value of K_0 is correct in order of magnitude (*International Critical Tables* 1927) but when the increase in thermal conductivity of organic liquids with pressure as found by Bridgman (1949) is taken into account, it is found to be approximately one-half of the value to be expected from Bridgman's results. At loads lower than 2×10^{8} dyn cm^{-1} the discrepancy is greater.

(iii) *The values of* δ

In figure 25 values of $\bar{\eta}_m$ deduced from the friction measurements of figure 21 are plotted against sliding speed. The figure also includes curves calculated for various values of K_0/γ.

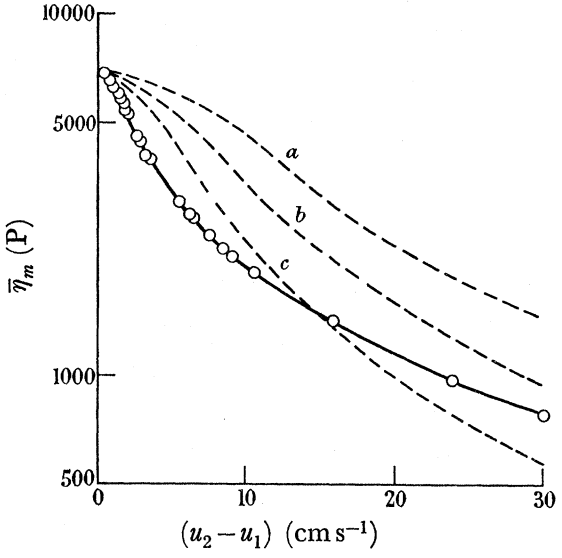

FIGURE 25. The variation of $\bar{\eta}_m$ with sliding speed up to a sliding speed of 30 cm s^{-1}. Load $= 1{\cdot}2\times10^{8}$ dyn cm^{-1}, $\bar{u} = 400$ cm s^{-1}, $\eta_s \simeq 1{\cdot}4$ P. —○—, From experiment; ----, calculated. (*a*) $K_0/\gamma = 1{\cdot}5\times10^{5}$ dyn s^{-1}; (*b*) $K_0/\gamma = 7{\cdot}5\times10^{4}$ dyn s^{-1}; (*c*) $K_0/\gamma = 3{\cdot}75\times10^{4}$ dyn s^{-1}.

When the value of K_0/γ is reduced the calculated curve falls more steeply as the sliding speed increases, but even for the curve where the implausible low value of $3{\cdot}75\times10^{4}$ dyn s^{-1} was taken for K_0/γ the calculated curve is less steep than the curve deduced from the experimental results. The most probable cause of the difference is that δ varies intrinsically (i.e. at constant temperature) as the sliding speed increases. If δ is a function of (u_2-u_1) equation (6·2) should be replaced by

$$\frac{K_0}{\gamma} = (u_2-u_1)^3\left[\frac{2\bar{\eta}_m}{(u_2-u_1)}+\frac{\partial\bar{\eta}_m}{\partial(u_2-u_1)}\right]\Big/\left[8+\frac{2F(u_2-u_1)}{b}\,\frac{\partial\delta}{\partial(u_2-u_1)}\right];$$

$\partial\delta/\partial(u_2-u_1)$ is negative so the result of taking the variation of δ into consideration will be values of K_0/γ greater than would otherwise be obtained. For instance, at a load of 2×10^{8} dyn cm^{-1} and a sliding speed of 350 cm s^{-1} a value of $\partial\delta/\partial(u_2-u_1)$ of -6×10^{-13} dyn^{-1} cm s would produce a value of K_0/γ of $3{\cdot}6\times10^{5}$ dyn s^{-1} and for $\gamma = 5\times10^{-3}$ deg C^{-1} a value of K_0 of $1{\cdot}8\times10^{4}$ dyn s^{-1} deg C^{-1}. This value of K_0 is consistent with Bridgman's results

(Bridgman 1949) and, as may be seen from table 3, the value of $\partial\delta/\partial(u_2-u_1)$ assumed above is not improbable.

Thus by taking the variation of δ into account the need to consider anomalous values of either K_0 or of γ is lessened, but clearly further work and additional procedures are required to determine K_0, γ and δ separately. Nevertheless, it is considered that the values of γ and of δ which have risen from the interpretation of the results are substantially correct. (The value of γ which has been arrived at is larger than that assumed in the numerical illustrations of part III. It is considered that the temperature rise on the median plane shown in figure 24 (b) is more realistic than the larger temperature rise shown illustratively in figure 13 (c) of part III.)

It may be seen from figure 25 that for the particular conditions of the figure the effect of sliding upon viscosity is appreciable at a sliding speed of 4 cm s^{-1}. With the film thickness at 2 μ that speed gives a strain rate of 2×10^4 s^{-1}.

It may be shown that in pure rolling such and greater rates of strain occur within the entry zone, and that the rates of strain increase as the rolling speed increases. Consequently the intrinsic effect of shear upon viscosity will influence film thickness and is a secondary effect, additional to that of transit time (§ 4 (d)), which will reduce the rate of rise of film thickness with rolling speed.

(c) *The temperatures on the median plane*

It has been shown that the calculated temperatures on the median plane are similar whether the rise in temperature at the surfaces of the disks is or is not taken into account (figure 24 b). Consequently at high speeds of sliding ($\psi \gg 1$) the temperatures on the median plane with reference to the temperature of the surfaces of the disks at entry is given by the expression

$$\theta_c \simeq \frac{\delta P}{\gamma}+\frac{1}{\gamma}\left[\ln\left(\frac{\eta_s\gamma}{8K_0}\right)+2\ln(u_2-u_1)\right]$$

which was developed in § 5 of part III.

Also, at high speeds of sliding,

$$\bar{\eta}_m \simeq \frac{4K}{b\gamma(u_2-u_1)^2}\left[\tfrac{1}{2}\delta F+2b\ln(u_2-u_1)+b\ln\left(\frac{\eta_s\gamma}{2K}\right)\right] \quad \text{(equation (7·7) of part III).}$$

It follows from these equations that $\bar{\theta}_c$, the mean value of θ_c averaged over the Hertzian width $2b$, is given in terms of the frictional traction T_s by

$$\bar{\theta}_c \simeq \frac{T_s h^*(u_2-u_1)}{8K_0 b}.$$

With the thermal conductivity of the oil known it is therefore a simple matter to deduce from measurements of friction and film thickness the mean temperature of the oil on the median plane of the film. For example, at a load of 2×10^8 dyn cm^{-1} ($b = 2\times10^{-2}$ cm) and at $(u_2-u_1) = 400$ cm s^{-1} T_s was 6×10^6 dyn cm^{-1} and h^* was 0·9 μ. With K_0 taken as 2×10^4 dyn s^{-1} deg C^{-1} equation (5·1) gives $\bar{\theta}_c = 70$ deg C. But even without the thermal conductivity known equation (5·1) is still useful in that it indicates in a simple way the

factors upon which oil temperature depends. Thus, if T_s is expressed as μF, and the proportionalities $b \propto \sqrt{F}$, $h^* \propto (\bar{u}\eta_s)^{\frac{1}{2}}$ are used then

$$\bar{\theta}_c \propto \frac{\mu(u_2-u_1)\,(F\bar{u}\eta_s)^{\frac{1}{2}}}{K_0},$$

where μ is the coefficient of friction and F is the load per unit face width.

7. Conclusion

The rolling friction has been measured and for loads within the elasto-hydrodynamic régime it has been shown that the frictional traction is independent of load and proportional to film thickness. The effective viscosity of the oil at the rolling point has been measured and it has been shown that the variations of viscosity, both for changes in pressure and in temperature, become less as the rolling speed is increased. This behaviour has been discussed in relation to visco-elasticity and it has been shown that a visco-elastic hypothesis agrees with the observed behaviour qualitatively in that it also predicts decreasing sensitivities to pressure and temperature as the time of transit of the oil through the conjunction of the disks becomes less. However, the values of elastic modulus required to account for the behaviour are less than those which have been deduced from observations of the propagation in a mineral oil of shear waves as generated by vibrating quartz crystals (Barlow & Lamb 1959). Consequently the explanation of the behaviour observed in disk experiments in terms of visco-elasticity can only be tentative. Nevertheless, a distinctive dynamic behaviour of the oil has been demonstrated and it has been shown that this contributes significantly to the way in which the thickness of the hydrodynamic film varies with speed of rolling.

Measurements of frictional traction up to a sliding speed of 400 $\mathrm{cm\,s^{-1}}$ have been described and from these measurements values of effective viscosity have been deduced. With relation to load, rolling speed, sliding speed and the viscosity of the oil at the surface temperature of the disks a considerable agreement between the observed behaviour of the oil and the behaviour predicted by the theory of friction developed in part III has been demonstrated. However, a close comparison of experiment and theory has demonstrated the viscous behaviour of the oil to be more complex than was assumed in the theory. So that the theory should be mathematically tractable it was assumed that viscosity varies exponentially both with temperature and pressure. Even under static conditions (times so long that time does not matter) these exponential dependencies are only rough approximations. But in addition to the dynamic effects already referred to the results obtained with sliding show that viscosity varies intrinsically (i.e. at constant temperature) with rate of strain. Nevertheless, despite the crudity of the theoretical framework it does give a useful account of the larger phenomena and it is possible, even though inelegant, to describe the actual behaviour of the oil in relation to temperature and pressure in terms of exponents which vary with circumstance.

Examination of the experimental results in relation to theory has underlined the importance of the thermal conductivity of the oil in relation to friction. The simplest of thermal considerations indicate its importance, but the fact is that although much attention is paid to the way in which the viscosities of oils vary with temperature little is paid to the thermal conductivities of oils although, in elasto-hydrodynamic situations (e.g. ball-races,

PHILOSOPHICAL TRANSACTIONS OF THE ROYAL SOCIETY A MATHEMATICAL, PHYSICAL & ENGINEERING SCIENCES

gears), the thermal conductivity appears in the expressions for friction along with the temperature dependence of viscosity.

The work which has been described demonstrates that in a lubrication system of a widespread type a mineral oil possesses significant dynamic characteristics in addition to those static characteristics which are matters of routine test. The measurements which have been made could, undoubtedly, with profit be further refined and should, perhaps more importantly, be extended to other oils, synthetics and composite materials. It is to be hoped that from such work more coherent interpretations will arise and different significances will be seen.

The author records his deep appreciation of the careful patient work of Mr B. Jones and Mr R. B. Hieatt with the apparatus and in making measurements. He also thanks Dr W. Hirst and his other colleagues for their continued interest, and Dr T. E. Allibone, C.B.E., F.R.S., Director of the Laboratory, for permission to publish this paper.

Appendix A. Measurements of film thickness with the four-disk machine

The thicknesses of the films in the four-disk machine were derived both from measurements of the total electrical capacitance between disks C and D (figure 3) and, with a central disk of glass which carried an evaporated chromium electrode (Crook 1961*c*), from the rate of change of capacitance between the electrode and one of the outer steel disks.

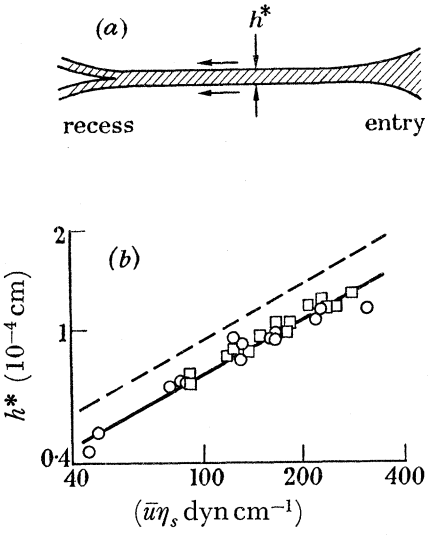

Figure 26. Measurements of film thickness (h^*) with the four-disk machine. (*a*) Oil filling between disks; (*b*) —○— from capacitance between steel disks, —□— from rate of change of capacitance between a steel disk and an electrode of evaporated chromium on a disk of glass, – – – – from pad measurements with two-disk machine (figure 3 (*a*) of part II).

The measurements of total capacitance between disks C and D were interpreted by calculating capacitance as a function of film thickness on the basis that the shape of the disks is Hertzian, that the entry zone is completely filled with oil and that at recess the oil divides as shown in figure 26 (*a*). The film thicknesses thereby deduced are plotted (circular points) as a function of $\bar{u}\eta_s$ in figure 26 (*b*); the thicknesses deduced from the experiments with a

central disk of glass are also shown (square points). The two sets of results are in close agreement.

The interrupted line in figure 26 (*b*) is from previous results (figure 3*a* of part II) derived from measurements by the pad method (part I) on disks nominally rolling in a two-disk machine. The present values lie beneath the line ($\sim 20\,\%$) as did those deduced from measurements of disk-disk capacitance in a two-disk machine (figure 8, part II) but the more important feature is that again film thickness is proportional to the half power of $\bar{u}\eta_s$. (It is to be expected that the pad method should give values greater than those based upon measurements pertaining to the conjunction itself because of the effects arising from the compressibility of the oil. The thickness given by the pad method should be reduced by the compression of the oil within the conjunction ($\sim 10\,\%$) while those derived from measurements pertaining to the conjunction should be increased proportionately with the increased dielectric constant of the compressed oil ($\sim 5\,\%$).)

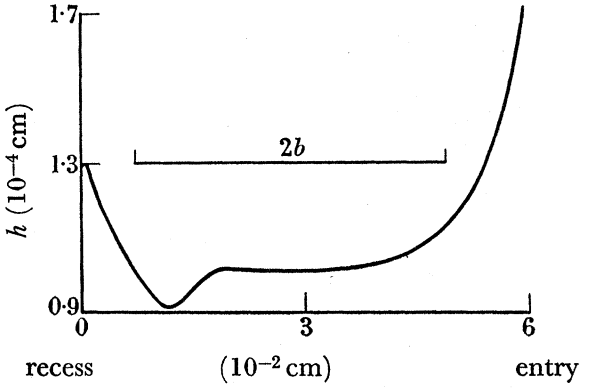

FIGURE 27. The shape of a conjunction. Load $= 8{\cdot}8 \times 10^7$ dyn cm^{-1}, $\bar{u} = 280$ cm s^{-1}.

By use of the glass disk with its electrode the shape of the oil film in cross-section may be deduced approximately and a typical result is given in figure 27. This provides direct confirmation that in the elasto-hydrodynamic régime the film thickness is constant to within approximately 10 % over the Hertzian band. It also shows directly the presence at recess of a constriction ($\sim 10\,\%$) in the oil film. Such a constriction is demanded by equation (4·2) for if P' is to fall to zero at the extreme recess somewhere beyond the point of maximum pressure $(h-h^*)$must become negative.

APPENDIX B. THE EFFECT UPON VISCOSITY OF THE TEMPERATURES DUE TO SMALL SPEEDS OF SLIDING

(*a*) *Viscosity at the surfaces of the disks*

The maximum rise in temperature at the surfaces of the disks ($\theta_{x\,\max.}$) due to the frictional heat flowing into them is given by (equation (9·5) of part III)

$$\theta_{x\,\max.} = \frac{0{\cdot}2T_s(u_2-u_1)}{(\pi K_D\rho_D c_D)^{\frac{1}{2}}\,(bu_{1,2})^{\frac{1}{2}}}\,[f(\beta)]_{\max.}, \quad [f(\beta)]_{\max.} = 1{\cdot}5,$$

where K_D, ρ_D and c_D are the thermal conductivity, density and specific heat of the material of the disks. With reference to curve *b* of figure 4 the extreme value of (u_2-u_1) is $\sim 0{\cdot}3$ cm s^{-1}, and for curve *a* it is $\sim 1{\cdot}2$ cm s^{-1}, while the values of T_s are respectively $\sim 1\times 10^5$

and $\sim 7\times10^4\,\mathrm{dyn\,cm^{-1}}$. In both instances $u_1 \simeq u_2 \simeq 300\,\mathrm{cm\,s^{-1}}$. The values of $\theta_{x\,\mathrm{max.}}$ are $2\times10^{-4}\,\mathrm{deg\,C}$ for curve b and $5\times10^{-4}\,\mathrm{deg\,C}$ for curve a ($\pi K_D\rho_D c_D$ taken as 5×10^{14} c.g.s. units).

The variation of viscosity with temperature will be taken as

$$\eta_\theta = \eta_0 \exp(-\gamma\theta),$$

where γ will be taken as $5\times10^{-2}\,^\circ\mathrm{C}^{-1}$. Consequently the effect of the temperature rise at the surfaces of the disks upon the viscosity at the surfaces (η_x) is negligible ($\ll 1\,\%$).

(*b*) *Viscosity within the oil film*

The effect of frictional heating can be assessed from the ratio of η_m/η_x as given by equation (7·4) of part III. That equation reduces to

$$\eta_m/\eta_x = (1-\tfrac{2}{3}\psi)$$

for small values of ψ where ψ is given by

$$\psi = \frac{\eta_x\gamma(u_2-u_1)^2}{8K_0} \qquad \text{(equation (5·9) of part III)}$$

K_0 is the thermal conductivity of the oil.

With reference to curve b of figure 4 the maximum value of η_x is approximately 1×10^5 P while $(u_2-u_1) \leqslant 0{\cdot}3\,\mathrm{cm\,s^{-1}}$. These values give

$$\eta_m/\eta_x \leqslant 0{\cdot}994$$

when $\gamma/8K_0$ is taken as $1\times10^{-6}\,\mathrm{dyn^{-1}\,s}$.

A similar calculation for curve a gives

$$\eta_m/\eta_x \leqslant 0{\cdot}997.$$

Therefore in these instances frictional heating depresses η_m by less than 1 %.

Appendix C. The heating due to compression

If the compression is thermodynamically reversible it follows from conservation of energy and Maxwell's relation

$$\left(\frac{\partial S}{\partial P}\right)_\theta = -\left(\frac{\partial V}{\partial \theta}\right)_P,$$

where S is entropy and V is volume that when the oil is subjected to an increment of pressure (ΔP) then an element of oil must transfer to its surroundings a quantity of heat per unit volume (ΔQ) where

$$\Delta Q = \theta\nu\,\Delta P - \rho_o c_o \Delta\theta,$$

θ is temperature but now in °K, ν is the coefficient of expansion of the oil (ν will be taken as $6\times10^{-4}\,^\circ\mathrm{C}^{-1}$), ρ_o is the density of the oil and c_o is its specific heat at constant pressure.

The compression will not be exactly reversible but the above relationship will be an adequate approximation.

If q is the rate of transfer of heat per unit volume

$$q = -\theta v\bar{u}\frac{\partial P}{\partial x} + \rho_o c_o \bar{u}\frac{\partial \theta}{\partial x}. \tag{C 1}$$

If there is no transfer (i.e. the heat flow is purely convective)

$$\rho_o c_o \frac{\partial \theta}{\partial x} = \theta v \frac{\partial P}{\partial x},$$

the solution is

$$\theta = \theta_s \exp(vP/\rho_o c_o), \tag{C 2}$$

where θ_s is the absolute temperature of the oil at entry.

If the transfer of heat is solely by conduction

$$K_0 \frac{\partial^2 \theta}{\partial y^2} = -q \quad \text{(equation (3·2) of part III)}. \tag{C 3}$$

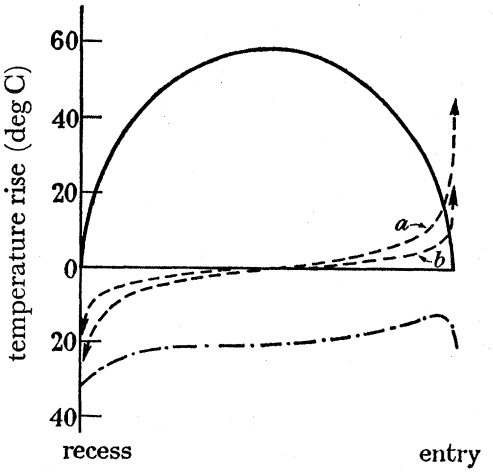

FIGURE 28. Heating due to compression; temperature rise to dissipate heat; ——, by convexion; – – – –, by conduction; (*a*) $\bar{u} = 1000\,\mathrm{cm\,s^{-1}}$; (*b*) $\bar{u} = 100\,\mathrm{cm\,s^{-1}}$, —·— diagrammatic curve of actual temperature rise (temperature origin shifted).

To assess the temperatures arising with conduction alone the second term on the left of equation (C 1) will be dropped. The solution of equation (C 3) is then

$$\theta_s/\theta_c = \cos\left[\frac{h^*}{2} \pm \sqrt{\left(\frac{\mp v\bar{u}}{K_0}\frac{\partial P}{\partial x}\right)}\right], \tag{C 4}$$

where θ_c is the absolute temperature on the median plane of the film.

In figure 28 the temperature rise in the oil film for the greatest load employed (2×10^8 dyn cm^{-1}) and a Hertzian distribution has been calculated both from equations (C 2) and (C 4).

If, over the central region of the Hertzian band the temperatures of convexion existed then it is clear from the figure that amounts of heat much greater than $\theta v\,\partial P/\partial x$ would be conducted away. Therefore over the central region the temperatures of conduction prevail and, in particular, equation (C 4) gives no rise in temperature at the mid point. (With respect to the curve for conduction $\rho_o c_o(\partial\theta/\partial x)$ is in general small compared with $\theta v(\partial P/\partial x)$.

Whatever temperatures exist away from the mid-point they are of lesser importance in their effect upon the value of $\bar{\eta}_m$ as they influence values of η_m which are falling to zero at entry and recess. Furthermore, downstream of the mid-point the temperature rise which occurs ahead of the mid-point is balanced by a fall. The associated increases and reductions in η_m will tend to leave $\bar{\eta}_m$ unchanged.

But the balance is slightly imperfect as at entry the pressure builds up gradually to merge with the Hertzian distribution whereas at recess it falls more in accord with that distribution. The effect of this asymmetry is illustrated in the lower curve of figure 28; the oil leaves the conjunction at a temperature lower than that at which it enters.

References

Barlow, A. J. & Lamb, J. 1959 *Proc. Roy. Soc.* A, **253**, 52.

Bridgman, P. W. 1949 *The physics of high pressure.* London: Bell.

Cameron, A. & Newman, A. D. 1953 *Proc. Conf. Steam Turbine Research and Development.* London: Institution of Mechanical Engineers.

Crook, A. W. 1958 *Phil. Trans.* A, **250**, 387 (part I).

Crook, A. W. 1961*a* *Phil. Trans.* A, **254**, 223 (part II).

Crook, A. W. 1961*b* *Phil. Trans.* A, **254**, 237 (part III).

Crook, A. W. 1961*c* *Nature, Lond.* **190**, 1182.

Crouch, R. F. & Cameron, A. 1960 *J. Inst. Petrol.* **46**, 119.

Grubin, A. N. 1949 Central Scientific Research Institute for Technology and Mechanical Engineering, book no. 30, Moscow. (D.S.I.R. translation.)

International Critical Tables 1927 **2**, 151. New York: McGraw Hill.

Mason, W. P., Baker, W. O., McSkimin, H. J. & Heiss, J. H. 1949 *Phys. Rev.* **75**, 936.

Milne, A. A. 1957 *Proc. Conf. on Lubrication and Wear*, p. 66. London: Institution of Mechanical Engineers.

Misharin, J. A. 1958 *Proc. Int. Conf. on Gearing*, p. 159. London: Institution of Mechanical Engineers.

Pressure Viscosity Report 1953 New York: Amer. Soc. Mech. Engrs.

Standard Viscosity-Temperature Chart 1939 Chart (D 341–43) C. Philadelphia: Amer. Soc. Testing Materials.

PHILOSOPHICAL TRANSACTIONS OF THE ROYAL SOCIETY A MATHEMATICAL, PHYSICAL & ENGINEERING SCIENCES